Editors' Suggestion

Fast high-fidelity single-qubit gates for flip-flop qubits in silicon

F. A. Calderon-Vargas,* Edwin Barnes, and Sophia E. Economou
Department of Physics, Virginia Tech, Blacksburg, Virginia 24061, USA

(Received 21 January 2022; accepted 20 September 2022; published 10 October 2022)

The flip-flop qubit, encoded in the states with antiparallel donor-bound electron and donor nuclear spins in silicon, showcases long coherence times, good controllability, and, in contrast to other donor-spin-based schemes, long-distance coupling. Electron spin control near the interface, however, is likely to shorten the relaxation time by many orders of magnitude, reducing the overall qubit quality factor. Here, we theoretically study the multilevel system that is formed by the interacting electron and nuclear spins and derive analytical effective two-level Hamiltonians with and without periodic driving. We then propose an optimal control scheme that produces fast and robust single-qubit gates in the presence of low-frequency noise without relying on parametrically restrictive sweet spots. This scheme increases considerably both the relaxation time and the qubit quality factor.

DOI: 10.1103/PhysRevB.106.165302

I. INTRODUCTION

Quantum computation promises to revolutionize the scientific world, from fundamental science to information technology [1]. In the ongoing race to build the first fully operational quantum computer, donor spin qubits in isotopically purified silicon (^{28}Si) [2] are promising candidates due to their long coherence times and their integrability with metal-oxide-semiconductor structures [3–9]. Donor spins present coherence times reaching around half a minute (half a second) for the nuclear (electron) spin [10,11], up to hours in bulk ensembles [12], and a high degree of controllability [13–15]. However, the implementation of two-qubit gates has proven to be quite challenging. Most of the approaches for two-qubit operations are based on Kane's seminal proposal [16], where the qubit coupling is achieved via the exchange interaction between donor-bound electrons. The use of such short-range interactions requires near-atomic precision in the placement of the donors [17,18]. And, even though recent works have shown more relaxed requirements on the precision of donor placement [19–21], long-distance coupling is still challenging without inserting intermediate couplers [22–24].

A recent proposal by Tosi *et al.* [25] circumvents the precise donor placement limitation by using the electric dipole, created when the electron is shared between the donor and the Si/SiO_2 interface, as a long-range coupling between a pair of qubits, each encoded in the flip-flop states of the donor-bound electron and donor nuclear spins. These qubits, hereafter called *flip-flop qubits*, can be fully controlled by microwave electric fields through hyperfine modulation. A constant (dc) electric field induces qubit rotations about the z axis, while an oscillating (ac) electric field implements x and y gates. The gate control of the electron near the interface, however, may cause flip-flop relaxation via spontaneous phonon emission, as shown in Ref. [26], resulting in a relaxation time T_1 approximately eight orders of magnitude shorter than in bulk [27], and a few orders of magnitude shorter than the T_1 predicted in Ref. [25]. This lowers the qubit quality factor (T_1/τ with τ being the qubit gate time), which gives the number of available qubit operations before coherence is lost. A high-quality factor is one of the main requirements for fault-tolerant quantum computing [28]. One way of improving the quality factor would be to increase T_1 by reducing the external magnetic field B_0 [25]. However, the magnetic field strength used in the experiments is usually between 0.4 T and 1.4 T. This is because the qubit readout via spin-dependent tunneling [29] requires the qubit Zeeman splitting to be larger than $\sim 5k_BT_e$, which is the thermal broadening of the electron reservoir at temperature T_e (usually between 100 mK and 200 mK) [30]. Therefore, lowering the magnetic field strength is not desirable. Another approach would be to use optimal control pulses that implement faster qubit gates in the magnetic field range used in the laboratory, which is the approach we take here.

In this paper, we propose optimally designed control pulses for fast high-fidelity single-qubit gates, i.e., arbitrary z and x rotations, for flip-flop qubits. We use both time-independent and time-dependent Schrieffer-Wolff (TDSW) transformations [31] to derive effective qubit Hamiltonians for both ac and dc driving. The former, required to implement x rotations, is studied in the strong driving regime using Floquet perturbation theory [32]. With the analytical effective qubit Hamiltonian, we are able to produce single-qubit gates that are much faster and more robust than previous proposals, with fidelities above 99.99%. Moreover, our scheme does not rely on restricting parameters to operational sweet spots, like clock transitions [25], allowing us, for example, to find fast gates for different magnetic fields strengths, increasing the relaxation time and the qubit quality factor considerably.

The paper is organized as follows. In Sec. II, we analyze the flip-flop qubit system and derive a simplified Hamiltonian in the combined spin and orbital eigenbases. Then, in

*Present address: Sandia National Laboratories, Livermore, California 94550, USA.

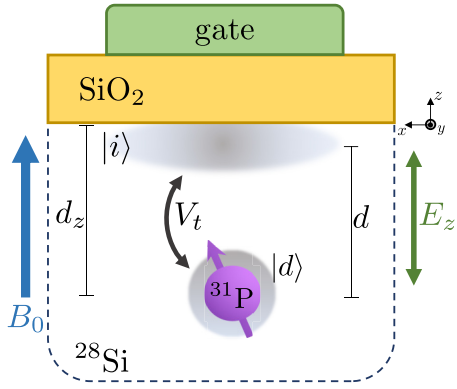

FIG. 1. Schematic of the flip-flop qubit system. A phosphorus donor is embedded in ^{28}Si at a depth d_z from the interface with a thin SiO_2 layer. A top metal gate controls the position of the wave function of the donor unpaired electron via an electric field E_z. The electron orbit is quantized into a $|d\rangle$ state at the donor and a $|i\rangle$ state at the interface. The wave functions of these states are schematically shown in gray.

Sec. III, we introduce an effective qubit Hamiltonian with no oscillating driving and use it to produce fast high-fidelity z rotations. In Sec. IV, we use TDSW perturbation theory (which is discussed in detail in Appendix A) to derive an effective two-level Hamiltonian with oscillating driving and, via Floquet perturbation theory, present analytical expressions for the resonance and Rabi frequencies, which are used to produce fast high-fidelity x rotations. We conclude in Sec. V.

II. SPIN AND ORBITAL HAMILTONIANS

The setup of the system follows the experimental proposal from Ref. [25], where the wave function of the donor-bound electron of a phosphorus donor (^{31}P) embedded in isotopically purified ^{28}Si is controlled by a vertical electric field E_z applied by a metal gate on top (Fig. 1). The donor is at a depth d_z from the interface with a thin SiO_2 layer. The electron (nuclear) spin $S = 1/2$ ($I = 1/2$) has a gyromagnetic ratio $\gamma_e/2\pi = 27.97$ GHz/T ($\gamma_n/2\pi = 17.23$ MHz/T) and basis states $\{|\uparrow\rangle, |\downarrow\rangle\}$ ($\{|\Uparrow\rangle, |\Downarrow\rangle\}$). For an isolated ^{31}P donor atom in unstrained Si, the isotropic Fermi-contact hyperfine interaction A in the nonrelativistic limit is proportional to the probability amplitude $|\psi(0,0,d_z)|^2$ of the unpaired electron wave function at the nucleus. Under a large magnetic field B_0 ($B_0(\gamma_e + \gamma_n) \gg A$) along the z axis, the spin Hamiltonian is

$$H_{\text{spin}} = \gamma_e B_0 S_z - \gamma_n B_0 I_z + A\vec{S}\cdot\vec{I}, \tag{1}$$

where $S_z = \frac{\hbar}{2}(|\uparrow\rangle\langle\uparrow| - |\downarrow\rangle\langle\downarrow|)$ ($I_z = \frac{\hbar}{2}(|\Uparrow\rangle\langle\Uparrow| - |\Downarrow\rangle\langle\Downarrow|)$) is the z component of the electron (nuclear) spin operator. The flip-flop states $\{|\uparrow\Downarrow\rangle, |\downarrow\Uparrow\rangle\}$ are effectively decoupled from the other states. Consequently, our analysis is henceforth focused on the Hilbert space spanned by the flip-flop states, but all the numerical results reported in thispaper are obtained keeping the full Hilbert space.

The shifting of the electron wave function by the electric field E_z creates an electric dipole $\mu_d = d\,e$, where e is the electron charge and d is the distance between the center-of-mass positions of the donor-bound ($|d\rangle$) and interface-bound ($|i\rangle$) orbitals (see Fig. 1). Following Ref. [25], we can use these two well-defined positions as two orthogonal quantum states, and describe the electron orbital dynamics with a simple two-level Hamiltonian:

$$H_{\text{orb}} = -\frac{d\,e\,\Delta E}{2\hbar}\tau_z^{id} + \frac{V_t}{2}\tau_x^{id}, \tag{2}$$

where $\Delta E = E_z - E_0$ is the deviation of the vertical electric field away from the ionization point E_0 (electric field value where the stationary electron charge is equally distributed between $|i\rangle$ and $|d\rangle$), V_t is the tunnel coupling between the orbital states $|i\rangle$ and $|d\rangle$, and $\tau_z^{id} = |i\rangle\langle i| - |d\rangle\langle d|$, $\tau_x^{id} = |i\rangle\langle d| + |d\rangle\langle i|$ are Pauli operators. In this paper, the qubit is operated with electric field E_z near the donor ionization field E_0 or $E_z < E_0$, where the valley splitting between the lower $|i\rangle$ and upper $|v\rangle$ valley interface states is much larger than the tunnel coupling V_t [25] and far from the anticrossing between $|d\rangle$ and $|v\rangle$.

Given the hyperfine dependence on the electron position, the hyperfine interaction $A(E)$ changes from the bulk value $A/2\pi \approx 117$ MHz to $A \approx 0$ when the electron is fully displaced to the interface. The electron gyromagnetic ratio also differs from its value at the donor when the electron is confined at the Si/SiO_2 interface; the difference Δ_γ can be up to 0.7% [25,33]. The orbital position dependence of these two energies can be incorporated in the Hamiltonian by treating them as projection operators in the orbital Hilbert space, i.e., $A(|d\rangle\langle d|)$ and $\gamma_e B_0 \Delta_\gamma |i\rangle\langle i|$.

The total Hamiltonian combines the spin and orbital degrees of freedom and, in the basis $\{|g\otimes\uparrow\Downarrow\rangle, |g\otimes\downarrow\Uparrow\rangle, |e\otimes\uparrow\Downarrow\rangle, |e\otimes\downarrow\Uparrow\rangle\}$, has the following form:

$$\begin{aligned} H = &-\frac{\varepsilon_0}{2}\sigma_{zi} + \frac{\varepsilon_z}{2}\sigma_{iz} + \frac{\Delta_{\varepsilon_z}}{4}(\sigma_{iz} + \sin\theta\,\sigma_{xz} + \cos\theta\,\sigma_{zz}) \\ &+ \frac{A}{8}(2\sigma_{ix} - 2\sin\theta\,\sigma_{xx} - 2\cos\theta\,\sigma_{zx} \\ &+ \sin\theta\,\sigma_{xi} + \cos\theta\,\sigma_{zi}), \end{aligned} \tag{3}$$

where $|g\rangle$ ($|e\rangle$) is the ground (excited) eigenstate of the orbital Hamiltonian Eq. (2), $\varepsilon_0 = \sqrt{(d\,e\,\Delta E/\hbar)^2 + V_t^2}$ and $\varepsilon_z = B_0(\gamma_e + \gamma_n)$ are the orbital and Zeeman energy splittings, $\Delta_{\varepsilon_z} = B_0\gamma_e\Delta_\gamma$ is the Zeeman energy shift when the electron is at the interface, $\tan\theta = V_t\hbar/(d\,e\,\Delta E)$ is a mixing angle, and $\sigma_{pq} = \tau_p \otimes \zeta_q$ is the Kronecker product of Pauli operators with $\sigma_{zz} = (|g\rangle\langle g| - |e\rangle\langle e|) \otimes (|\uparrow\Downarrow\rangle\langle\uparrow\Downarrow| - |\downarrow\Uparrow\rangle\langle\downarrow\Uparrow|)$.

The Hamiltonian acquires a simpler form in the basis formed by the orbital and hyperfine eigenstates, $\{|*\rangle\, g\,\widetilde{\uparrow\Downarrow}, |*\rangle\, g\,\widetilde{\downarrow\Uparrow}, |*\rangle\, e\,\widetilde{\uparrow\Downarrow}, |*\rangle\, e\,\widetilde{\downarrow\Uparrow}\}$. In this basis, the spin energy splitting is conditioned on the orbital state and is given by $\varepsilon_{s^{(\mp)}} = \sqrt{(A(1 \mp \cos\theta)/2)^2 + (\varepsilon_z + \Delta_{\varepsilon_z}(1 \pm \cos\theta)/2)^2}$, where $(-)$ and $(+)$ corresponds to the orbital ground and excited eigenstates, respectively. Owing to the orbital (ε_0), Zeeman (ε_z), and spin energy splittings being much larger than the hyperfine interaction (A) and Zeeman energy shift (Δ_{ε_z}), we neglect terms of the form η/ε where $\eta \in \{A, \Delta_{\varepsilon_z}\}$ and $\varepsilon \in \{\varepsilon_0, \varepsilon_z, \varepsilon_{s^{(\mp)}}\}$. The simplified Hamiltonian in the basis

$\{|*\rangle\, g\, \widetilde{\uparrow\Downarrow}, |*\rangle\, g\, \widetilde{\downarrow\Uparrow}, |*\rangle\, e\, \widetilde{\uparrow\Downarrow}, |*\rangle\, e\, \widetilde{\downarrow\Uparrow}\}$ is

$$\tilde{H} = \begin{pmatrix} -\frac{\varepsilon_0-\varepsilon_{s(-)}}{2} + \frac{A\cos\theta}{8} & 0 & \frac{(A+2\Delta_{\varepsilon_z})\sin\theta}{8} & -\frac{A\sin\theta}{4} \\ 0 & -\frac{\varepsilon_0+\varepsilon_{s(-)}}{2} + \frac{A\cos\theta}{8} & -\frac{A\sin\theta}{4} & \frac{(A-2\Delta_{\varepsilon_z})\sin\theta}{8} \\ \frac{(A+2\Delta_{\varepsilon_z})\sin\theta}{8} & -\frac{A\sin\theta}{4} & \frac{\varepsilon_0+\varepsilon_{s(+)}}{2} - \frac{A\cos\theta}{8} & 0 \\ -\frac{A\sin\theta}{4} & \frac{(A-2\Delta_{\varepsilon_z})\sin\theta}{8} & 0 & \frac{\varepsilon_0-\varepsilon_{s(+)}}{2} - \frac{A\cos\theta}{8} \end{pmatrix}. \tag{4}$$

The flip-flop qubit is encoded in the two lowest-energy eigenstates of the total Hamiltonian, which are approximately $|*\rangle\, g\, \widetilde{\downarrow\Uparrow}$ and $|*\rangle\, g\, \widetilde{\uparrow\Downarrow}$. The eigenenergies of the system Hamiltonian are shown in Fig. 2(a). Note that the qubit states $\{|0\rangle, |1\rangle\}$ are effectively $\{|g\downarrow\Uparrow\rangle, |g\uparrow\Downarrow\rangle\}$ for $\Delta E \gg 0$ ($\theta \approx 0$), which corresponds to fully displacing the electron to the interface. Moreover, at $|\Delta E| \gg 0$ ($\theta \approx \{0, \pi\}$) the electron is fully displaced either to the interface or to the donor, and as the flip-flop qubit is effectively decoupled from electric fields, these are referred to as idling regions. Conversely, the electron must be displaced to the region around the ionization point $\Delta E = 0$ ($\theta = \pi/2$) to implement any quantum gate. This is also the region, however, where the qubit is most sensitive to electrical noise and leakage. The latter can be reduced by applying slow-varying pulses to retain adiabaticity. The main source of noise in this type of system is charge noise, usually stemming from defects and electron traps at the Si/SiO_2 interface. Given that the qubit gates for donor qubits take less than a microsecond, the charge noise is usually static within a single gate and, therefore, we can model it as quasistatic noise. For this noise, Ref. [25] shows the presence of clock transitions in the flip-flop transition energy, i.e., regions where the transition is noise insensitive up to a certain order. This is clearly shown in Fig. 2(b), where, for a specific set of parameters, a second-order clock transition is found at $\Delta E \approx 0.4$ kV m^{-1}. However, as we will show in the following sections, it is possible to implement robust rotations that do not use the clock transition as an operating point. This can soften experimental requirements and improve the quality of gates at the same time.

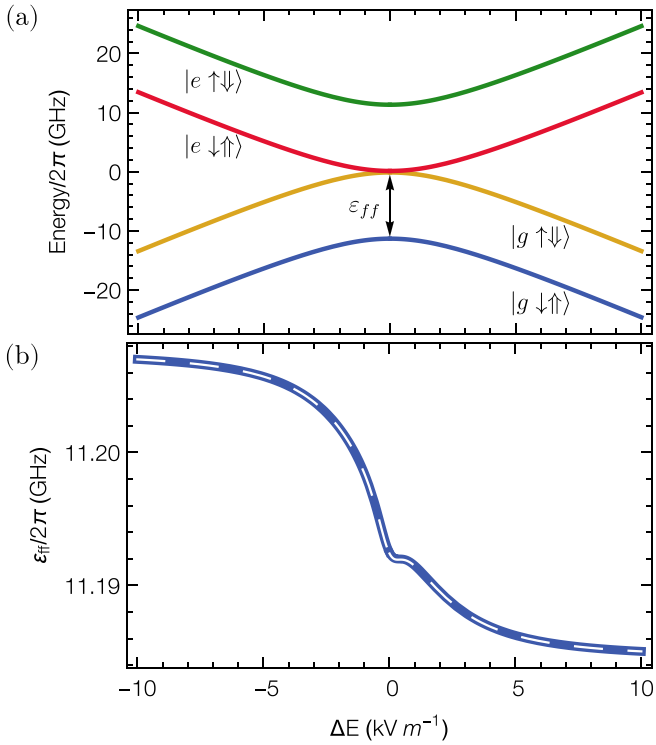

FIG. 2. (a) Energy-level diagram of the flip-flop system. The flip-flop qubit is encoded in the two lowest-energy eigenstates, with ε_{ff} being the transition energy between the two qubit levels. Moreover, note that for $E_z \gg E_0$ ($\Delta E \gg 0$) the qubit states $|0\rangle$ and $|1\rangle$ are effectively equal to the states $|g\downarrow\Uparrow\rangle$ and $|g\uparrow\Downarrow\rangle$, respectively. Similarly, for $E_z \ll E_0$ ($\Delta E \ll 0$) the excited levels are effectively equal to $|e\downarrow\Uparrow\rangle$ and $|e\uparrow\Downarrow\rangle$. (b) The numerically calculated transition energy ε_{ff} (blue curve), where the kink in the curve near $\Delta E = 0$ is the clock transition (reduced dephasing). The white dashed curve overlaying the blue one is obtained with the analytical expression for the effective flip-flop transition energy ε_{ff}, Eq. (7), showing excellent agreement with the numerical result. The system parameters used to plot both figures are $B_0 = 0.4$ T, $V_t/2\pi = 11.44$ GHz, $d = 15$ nm, and $\Delta_\gamma = -0.002$.

Donor spin qubits are among the most coherent solid-state quantum systems, and the flip-flop qubit is not expected to be an exception [25]. Nonetheless, a theoretical description [26] of the phonon-mediated relaxation of the flip-flop qubit shows that when the electron is at the ionization point ($\Delta E = 0$), the flip-flop relaxation time T_1 is a few orders of magnitude shorter than what Ref. [25] predicts and around eight orders of magnitude shorter than what was predicted for a P donor in bulk silicon [27]. This can be counteracted, however, by increasing the tunnel coupling V_t which, according to Tosi *et al.*'s proposal [25], should be able to be tuned by at least two orders of magnitude. Evidently, the ratio $T_1^{(i)}/T_1^{(j)}$ (i, j referring to two different sets of system parameters) given by [26]

$$\frac{T_1^{(i)}}{T_1^{(j)}} = \left[\frac{\varepsilon_0^2\left(\varepsilon_0^2 - (\gamma_e B_0)^2\right)^2}{V_t^4(\gamma_e B_0)^3}\right]^{(i)} \left[\frac{V_t^4(\gamma_e B_0)^3}{\varepsilon_0^2\left(\varepsilon_0^2 - (\gamma_e B_0)^2\right)^2}\right]^{(j)}, \tag{5}$$

with $\varepsilon_0 = \sqrt{(d\, e\, \Delta E/\hbar)^2 + V_t^2}$, shows that increasing the tunnel coupling in (i) relative to (j) and keeping the other parameters equal does indeed increase the relaxation time of (i) with respect to (j). In the following sections, we show that it is possible to implement fast high-fidelity single-qubit gates with different magnetic field strengths and tunnel coupling values, improving the qubit quality factor.

For the analysis and results reported in this paper, unless stated otherwise, we use the same parameters reported in Ref. [25]. Accordingly, the distance d is equal to 15 nm, and $\Delta_\gamma = -0.002$.

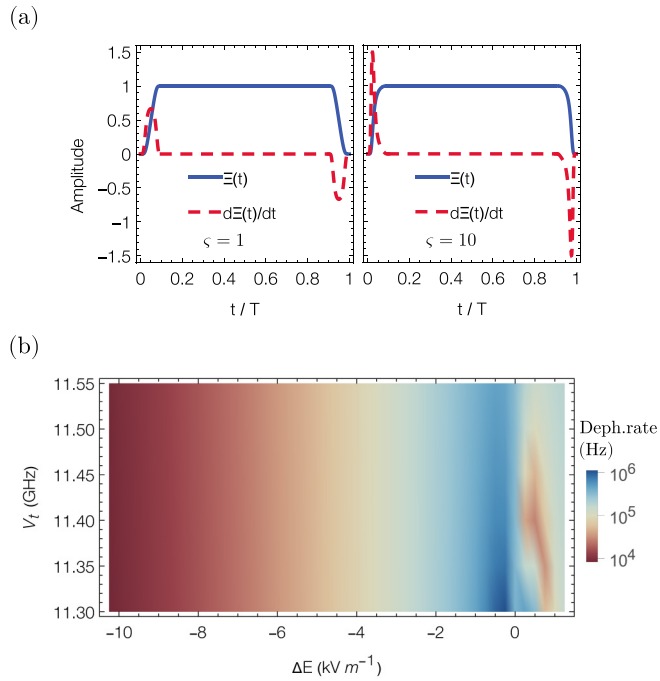

FIG. 3. (a) Example of a pulse using Eq. (6) with arbitrary parameters. The pulses (solid blue curves) in both panels have the same ramp time $t_r/T = 0.1$ (and same gate time T) but different values for ς. Note that for larger ς, the pulse slope of the region between the inflection point and the plateau is lowered, which is evidenced by the pulse first derivative curve (dashed red line). The pulse first derivative curves in both panels are reduced in amplitude for visualization purposes. (b) Estimated flip-flop qubit dephasing rate, assuming electric field noise $\delta E_{z,\mathrm{rms}} = 100$ V m^{-1}. In the region around $\Delta E = 10$ kV m^{-1} and also at $\Delta E \approx 0.4$ kV m^{-1} (clock transition), the qubit dephasing rate is at least two orders of magnitude smaller than near the ionization point $\Delta E = 0$.

III. $R_z(\phi)$ GATES AND EFFECTIVE HAMILTONIAN WITHOUT OSCILLATING DRIVING

Qubit rotations about the z axis in the flip-flop system are implemented by displacing the electron from an idling point ΔE_{idle} (preferably near the interface where the hyperfine interaction is effectively null) toward an operating point ΔE_{op} in the region around the ionization point, parking there for a certain amount of time, and then returning to the initial point ΔE_{idle}. We consider two operating points, one at the clock transition $\Delta E = 0.4$ kV m^{-1} (as proposed in Ref. [25]), and the other beyond the ionization point and closer to the donor ($\Delta E = -12$ kV m^{-1}), both under the same magnetic field strength, $B_0 = 0.4$ T, and tunnel coupling, $V_t/2\pi = 11.44$ GHz. We also consider larger magnetic fields and larger tunnel couplings, $\{B_0 = 0.8\ \mathrm{T}, V_t/2\pi = 22.55\ \mathrm{GHz}\}$ and $\{B_0 = 1.2\ \mathrm{T}, V_t/2\pi = 33.71\ \mathrm{GHz}\}$, both with operating points closer to the donor, $\Delta E = -20$ kV m^{-1} and $\Delta E = -30$ kV m^{-1}, respectively. The operating points closer to the donor produce high-fidelity gates but are not unique: any operating point closer to the donor could also produce high-fidelity gates. This is because in that region the flip-flop qubit dephasing rate is much lower than near the ionization point. As shown in Fig. 3(b), the dephasing rate in the region closer to the donor is as low as or lower than the dephasing rate at the second order clock transition. Now, if ΔE_{op} is too close to the ionization point ($\Delta E = 0$), the applied electric field must vary slowly when approaching the fast dephasing region around the ionization point to preserve adiabaticity and avoid leakage to unwanted excited states. This can be accomplished with a smooth pulse, a modified Planck-taper window function [34]:

$$\Xi(t) = \xi_0 + \begin{cases} \frac{\xi_f - \xi_0}{1+\exp[\frac{t_r}{t} + \frac{t_r}{t-t_r}]/\varsigma} & t_0 < t < t_r \\ \xi_f - \xi_0 & t_r \leqslant t \leqslant (T - t_r) \\ \frac{\xi_f - \xi_0}{1+\exp[\frac{-t_r}{t-T+t_r} - \frac{t_r}{t-T}]/\varsigma} & (T - t_r) < t < T \\ 0 & t \leqslant t_0 \text{ or } t \geqslant T. \end{cases} \tag{6}$$

Here, t_0 is the time at the start of the pulse, t_r is the ramp time, T is the gate time ($T > 2t_r$), ξ_0 is the value of the control field at the start and end of the pulse, ξ_f is the control field value at the pulse plateau, and $\varsigma > 0$ modulates the pulse slope such that for $\varsigma > 1$ it is decreased in the region between the pulse inflection points and plateau, see Fig. 3(a). The latter is useful for preserving the adiabaticity when the pulse plateau is in a region in close proximity to excited states. For the control of the donor electron position, we use $\xi_0 = \Delta E_{\mathrm{idle}} \gg 0$ such that the electron is at or near the interface and $\xi_f = \Delta E_{\mathrm{op}}$ is the electric field magnitude that places the electron at the operating point.

The amount of time the electron should remain parked at the operating point to implement some desired qubit rotation can be determined with an analytic effective Hamiltonian in the qubit logical space. Noting that the off-diagonal elements of the Hamiltonian Eq. (4) are smaller than the diagonal ones, we use a TDSW transformation [31] (aka van Vleck or quasidegenerate perturbation theory [35–37]; see Appendix A) up to fourth order to diagonalize the Hamiltonian Eq. (4). We consider up to fourth order because we will need an expression for the transition energy as precise as possible to find the optimum conditions to generate high-fidelity $R_x(\phi)$ rotations with an oscillating magnetic field. Note that the off-diagonal elements are non-negligible only near the ionization point $\Delta E = 0$ ($\theta = \pi/2$), and in this region the orbital-conditioned spin energy splittings are effectively equal ($\varepsilon_{s^{(-)}} \approx \varepsilon_{s^{(+)}}$), which is assumed in the SW transformation. The resulting effective Hamiltonian in the qubit space is $H_{\mathrm{ff}} = -\frac{1}{2}\varepsilon_{\mathrm{ff}}\sigma_z$ (with $\sigma_z = |0\rangle\langle 0| - |1\rangle\langle 1|$) and the flip-flop transition energy $\varepsilon_{\mathrm{ff}}$ is given by

$$\varepsilon_{\mathrm{ff}} = \varepsilon_{s^{(-)}} - A\sin^2\theta\left(\frac{\Delta_{\varepsilon_z}}{8\varepsilon_0} + \frac{A\varepsilon_{s^{(-)}}}{8\Delta_{os}^2} \times \frac{A^2\varepsilon_0\varepsilon_{s^{(-)}}\cos\theta}{16\Delta_{os}^4} - \frac{A^3\varepsilon_0^2\varepsilon_{s^{(-)}}\sin^2\theta}{32\Delta_{os}^6}\right), \tag{7}$$

where $\Delta_{os}^2 \equiv \varepsilon_0^2 - \varepsilon_{s^{(-)}}^2$. Figure 2(b) shows excellent agreement between the analytical expression for the flip-flop transition and the numerical result.

The magnitude of $\varepsilon_{\mathrm{ff}}/2\pi$ in the idling region ($\Delta E \gg 1$) is on the order of GHz, therefore, to have an identity operation when the electron is at the idling point ΔE_{idle}, we move to a frame rotating with a frequency equal to the flip-flop qubit precession frequency at the idling point. Therefore, the evolution operator in this frame is $\tilde{U}(t, t_0) = U_0^\dagger(t, t_0)U(t, t_0)$. Here, $U(t, t_0) = \mathcal{T}\{\exp(-i\int_{t_0}^{t} H(\tau)\mathrm{d}\tau)\}$ is the evolution

operator with the time-dependent Hamiltonian given by Eq. (3) and $U_0(t,t_0)=\exp(-iH_0(t-t_0))$ is the evolution operator with the time-independent Hamiltonian $H_0 \equiv H(\Delta E_{\rm idle}) = -\frac{1}{2}\varepsilon_{s^{(-)}}(\Delta E_{\rm idle})\sigma_z$, where the constant $\Delta E_{\rm idle}$ is chosen such that $\theta \approx 0$ in Eq. (3). Then the donor electron displacement from the idling point to the operating point implements a rotation about the z axis with an angle (phase accumulated) given by

$$\phi = -\int_{t_0}^{t} (\varepsilon_{\rm ff}(\tau) - \varepsilon_{s^{(-)}}(\Delta E_{\rm idle}))d\tau. \tag{8}$$

We use Eq. (8) and the average gate fidelity to numerically find the ramp and gate times for the control pulse Eq. (6) that produces a high-fidelity z rotation about some target angle. The average gate fidelity is defined as [38]

$$\mathcal{F} = \frac{1}{m(m+1)}(\mathrm{Tr}[\tilde{U}\tilde{U}^\dagger] + |\mathrm{Tr}[\mathcal{U}^\dagger\tilde{U}]|^2), \tag{9}$$

where m is the dimension of both evolution operator $\tilde{U}$ and target operation $\mathcal{U}$. We find that using $\xi_0 = \Delta E_{\rm idle} = 60$ kV m^{-1} and $\xi_f = \Delta_{\rm op} = 0.4$ kV m^{-1}, i.e., the idling point is near the interface and the operating point is at the clock transition, a π z rotation can be generated in $T = 70.35$ ns with a ramp time $t_r = 4.3$ ns and $\varsigma = 70$. The fidelity of this rotation in the absence of noise is 99.999%. This is similar to the result for a π z gate shown in Ref. [25] (it is not exactly equal because we use a slightly different control pulse). Alternatively, using the same idling point but a different operating point closer to the donor [39], $\Delta E_{\rm op} = -12$ kV m^{-1}, we can implement a π z rotation with the same fidelity (in the absence of noise) as before but with a much shorter gate time $T = 23$ ns ($t_r = 0.9$ ns and $\varsigma = 1$). Figure 4(a) shows that with the same pulse parameters, we can implement fast high-fidelity z rotations by any arbitrary angle.

Charge noise is the main source of decoherence in quantum devices based on isotopically purified silicon (^{28}Si), and it can be caused by nearby charge fluctuators [40]. Other sources of noise, e.g., Johnson-Nyquist noise and high-frequency noise due to voltage noise at the metallic gates, are expected to be negligible or can be effectively suppressed via hardware modifications like inserting low-temperature attenuation along the high-frequency lines, which ensures the metal gates are well thermalized and substantially attenuates the noise of the room-temperature electronics [25]. Charge noise typically has a power spectral density that varies approximately as $1/f$ over a large range of frequencies f. In the flip-flop system, charge noise introduces electrical fluctuations that affect the control electric field $E_z(t)$. The tunnel coupling V_t can also be affected by overlap variations between the donor and interface wave functions due to fluctuations on the interface potential landscape, which can be caused by gate voltage noise or other sources of charge noise. Owing to the large low-frequency component of the noise spectrum, a general approach for handling this type of noise influence on the system is to treat the voltage noise and the averaged collective effect of the nearby charge fluctuators as quasistatic perturbations, i.e., the noise is assumed constant during the gate time. Accordingly, we calculate the gate infidelity $1-\mathcal{F}$, Eq. (9), of some of the gates reported above for different strengths of the electric

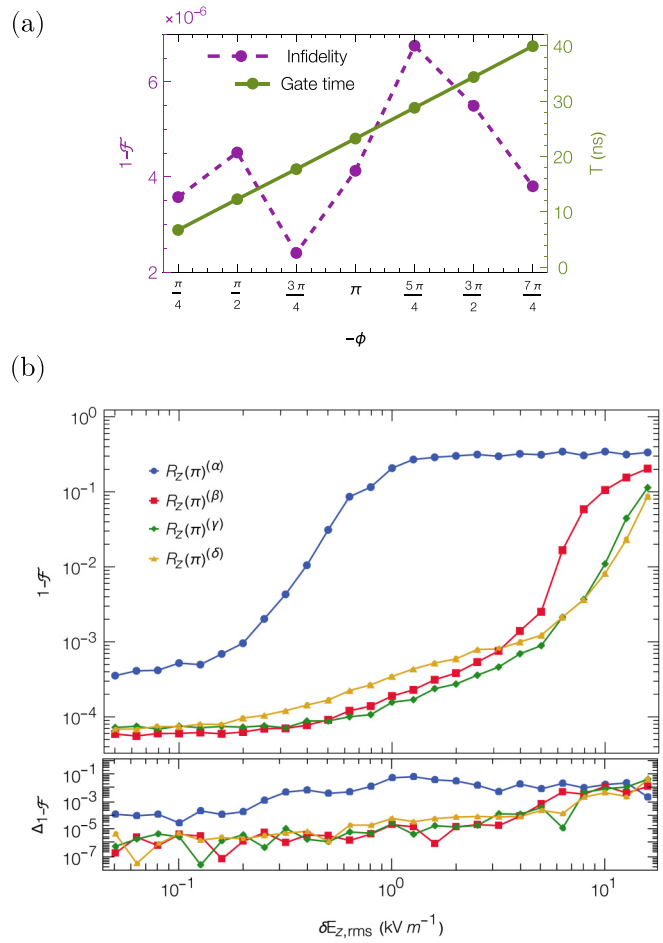

FIG. 4. (a) Infidelity, $1-\mathcal{F}$ Eq. (9), in the absence of noise, and gate times for z rotations about different angles. The pulse parameters used are $\xi_0 = 60$ kV m^{-1}, $\xi_f = -12$ kV m^{-1}, $t_r = 0.9$ ns, and $\varsigma = 1$. The infidelity for each rotation is on the order of 10^{-6}, and the relative variation between rotation infidelities is solely due to fluctuations in the convergence of the numerical search algorithm for increasing integration times. Finally, note that $R_z(-\phi) \equiv \exp[i\phi\sigma_z/2]$ is equivalent to $e^{i\pi}R_z(\varphi) \equiv e^{i\pi}\exp[-i\varphi\sigma_z/2]$, where $\varphi \equiv 2\pi - \phi$. (b) Upper part: Infidelity of π z rotations as a function of various electric field noise strength values $\delta E_{z,\rm rms}$ and fixed tunnel coupling noise $\delta V_{t,\rm rms}$. The tunnel coupling noise and pulse parameters for each gate are given in Table I. Lower part: Change in infidelity $\Delta_{1-\mathcal{F}}$ between gate infidelity obtained with only electric field noise δE_z and gate infidelity obtained with noise on both electric field δE_z and tunnel coupling δV_t.

field noise $\delta E_{z,\rm rms}$ and a fixed tunnel coupling noise amplitude $\delta V_{t,\rm rms}$. The latter is estimated from the simulation data for V_t as a function of the top metal gate voltage V_r presented in Fig. 2(g) of Ref. [25]. We assume a 10 μV rms noise [25,41] in V_r to estimate $\delta V_{t,\rm rms}$. The upper part of Fig. 4(b) shows π z-rotation infidelities averaged over the strength of the quasistatic electric field and tunnel coupling noises by sampling random perturbations δE_z and δV_t (linearly added to $\Delta E(t)$ and V_t, respectively) over uniform distributions with range $\sqrt{3}[-\delta E_{z,\rm rms}, \delta E_{z,\rm rms}]$ and $\sqrt{3}[-\delta V_{t,\rm rms}, \delta V_{t,\rm rms}]$. The average is taken over 200 samples for each value of $\delta E_{z,\rm rms}$, ranging from 0.05 kV m^{-1} and 19.95 kV m^{-1}, and 200 samples for

TABLE I. System and pulse parameters for each infidelity curve in Fig. 4(b). For each curve, the stated average gate fidelity $\mathcal{F}$ is calculated assuming electric field noise $\delta E_{z,\mathrm{rms}} = 100$ V m^{-1} and tunnel coupling noise $\delta V_{t,\mathrm{rms}}$ indicated in this table.

	$R_z(\pi)^{(\alpha)}$	$R_z(\pi)^{(\beta)}$	$R_z(\pi)^{(\gamma)}$	$R_z(\pi)^{(\delta)}$
B_0 (T)	0.4	0.4	0.8	1.2
$V_t/2\pi$ (GHz)	11.44	11.44	22.55	33.71
ΔE_{op} (kVm^{-1})	0.4	−12	−20	−30
t_r	4.3	0.9	0.9	0.8
ς	70	1	1	1
$\delta V_{t,\mathrm{rms}}/2\pi$ (MHz)	2.7	2.7	3.3	3.5
T (ns)	70.35	23	12.36	24.04
$\mathcal{F}$ (%)	99.95	99.994	99.992	99.993

the value of $\delta V_{t,\mathrm{rms}}$ in Table I associated to each z rotation. The lower part of Fig. 4(b) presents the change in infidelity $\Delta_{1-\mathcal{F}}$ when only electric field noise is taken into account. This shows that the impact of the tunnel coupling noise on the gate infidelity is, on average, an order of magnitude lower than the estimated infidelity when only electric field noise is considered, e.g., if $1-\mathcal{F}$ is on the order of 10^{-4} with only electric field noise, then including the tunnel coupling noise in the calculation would modify $1-\mathcal{F}$ on the order of 10^{-5} or less. Now, in the particular case of the flip-flop system, Ref. [25] estimates that the rms amplitude of the quasistatic electric field noise affecting the system along the z axis is $\sim$100 V m^{-1}. In Fig. 4(b), the first curve $R_z(\pi)^{(\alpha)}$, which has the clock transition as the operating point, presents a $\sim$99.95% fidelity at $\delta E_{z,\mathrm{rms}} = 0.1$ kV m^{-1} and $\delta V_{t,\mathrm{rms}}/2\pi = 2.7$ MHz, and a gate time of $T = 70.35$ ns. The overall fidelity, however, can be bumped up by choosing an operating point even closer to the donor. For example, $R_z(\pi)^{(\beta)}$ in Fig. 4(b) is generated by a pulse Eq. (6) with an operating point closer to the donor $\xi_f = \Delta E_{\mathrm{op}} = -12$ kV m^{-1} and has a 99.994% fidelity under realistic noise amplitudes $\delta E_{z,\mathrm{rms}} = 0.1$ kV m^{-1} and $\delta V_{t,\mathrm{rms}}/2\pi = 2.7$ MHz, and a much shorter gate time $T = 23$ ns. Fast high-fidelity gates can also be produced with a stronger magnetic field and an operating point closer to the donor, e.g., the third curve in Fig. 4(b) $R_z(\pi)^{(\gamma)}$ has $\Delta E_{\mathrm{op}} = -20$ kV m^{-1} as the operating point and a magnetic field $B_0 = 0.8$ T; it has a 99.992% fidelity and a gate time $T = 12.36$ ns at the noise amplitudes $\delta E_{z,\mathrm{rms}} = 0.1$ kV m^{-1} and $\delta V_{t,\mathrm{rms}}/2\pi = 3.3$ MHz, which is much shorter than the gate with the clock transition as the operating point. Similarly, for a magnetic field $B_0 = 1.2$ T we predict π z rotations with a 99.993% fidelity and a gate time $T = 24.04$ ns at the noise amplitudes $\delta E_{z,\mathrm{rms}} = 0.1$ kV m^{-1} and $\delta V_{t,\mathrm{rms}}/2\pi = 3.5$ MHz. Finally, for each z rotation in Fig. 4(b), we find that variations in the control pulse length of less than ± 0.1 ns have a negligible effect on the fidelity, but variations greater than ± 0.2 ns can reduce the fidelity by at least one order of magnitude (see Appendix E for more details).

The use of an operating point closer to the donor results in faster and high-fidelity z rotations because of the relative magnitude and shape of the flip-flop transition energy $\varepsilon_{\mathrm{ff}}$ as it gets closer to the donor (see Fig. 2). In this region, the magnitude of $\varepsilon_{\mathrm{ff}}$ is larger than its value at the clock transition, which speeds up the rotation [see Eq. (8)] and raises the qubit quality factor. Also, its slope ($\partial_{\Delta E}\varepsilon_{\mathrm{ff}}$) decreases as it gets closer to the donor and the time spent near the ionization point is minimal, factors which combine to minimize the dephasing errors. Another advantage of using smooth pulses and ΔE_{op} closer to the donor is that fast high-fidelity z-] rotations can be generated with rather low tunnel coupling values. In Appendix D, we show numerical results demonstrating that with tunnel couplings of just a few GHz, it is possible to generate fast high-fidelity R_z gates in the presence of noise. Moreover, without the need of a clock transition, there is more freedom to explore different sets of parameters that may lead to an overall better qubit performance. This has a direct impact on the relaxation time, since using an operating point closer to the donor increases the magnitudes of both ε_0 and T_1 considerably. For example, for $B_0 = 0.4$ T and $V_t = 11.44$ GHz, using $\Delta E_{\mathrm{op}} = -12$ kV m^{-1} as the operating point instead of the clock transition $\Delta E_{\mathrm{op}} = 0.4$ kV m^{-1} increases the relaxation time five orders of magnitude.

IV. $R_x(\phi)$ GATES AND EFFECTIVE HAMILTONIAN WITH OSCILLATING DRIVING

The implementation of an x rotation about an arbitrary angle [$R_x(\phi)$] requires the use of an oscillating electric field to drive transitions between the flip-flop qubit states. The electric field, then, is given by $\Delta E(t) = \Delta E^{(\mathrm{dc})}(t) + E^{(\mathrm{ac})}(t)\cos(\omega t + \varphi)$, where $\Delta E^{(\mathrm{dc})}(t)$ [$E^{(\mathrm{ac})}(t)$] is the dc (ac) amplitude of the electric field. The use of an oscillating field incorporates the following energy term to the system Hamiltonian [Eq. (3)]:

$$H_{\mathrm{orb}}^{(\mathrm{ac})} = -\frac{\varepsilon_{\mathrm{ac}}}{2}\cos(\omega t + \varphi)(\sin\theta\,\sigma_{xi} + \cos\theta\,\sigma_{zi}), \tag{10}$$

where $\varepsilon_{\mathrm{ac}} = d\,e\,E^{(\mathrm{ac})}/\hbar$. In the basis $\{|*\rangle\, g\, \widetilde{\uparrow\Downarrow}, |*\rangle\, g\, \widetilde{\downarrow\Uparrow}, |*\rangle\, e\, \widetilde{\uparrow\Downarrow}, |*\rangle\, e\, \widetilde{\downarrow\Uparrow}\}$, the simplified Hamiltonian Eq. (4) with ac driving has the following form:

$$\tilde{H}^{(\mathrm{ac})} = \begin{pmatrix} \frac{-(\varepsilon_0-\varepsilon_{s(-)})}{2} + \Lambda(t)\cos\theta & 0 & \Phi^{(+)}(t)\sin\theta & -\frac{1}{4}A\sin\theta \\ 0 & \frac{-(\varepsilon_0+\varepsilon_{s(-)})}{2} + \Lambda(t)\cos\theta & -\frac{1}{4}A\sin\theta & \Phi^{(-)}(t)\sin\theta \\ \Phi^{(+)}(t)\sin\theta & -\frac{1}{4}A\sin\theta & \frac{(\varepsilon_0+\varepsilon_{s(+)})}{2} - \Lambda(t)\cos\theta & 0 \\ -\frac{1}{4}A\sin\theta & \Phi^{(-)}(t)\sin\theta & 0 & \frac{(\varepsilon_0-\varepsilon_{s(+)})}{2} - \Lambda(t)\cos\theta \end{pmatrix}, \tag{11}$$

where $\Lambda(t) = \frac{1}{8}A - \frac{1}{2}\varepsilon_{\mathrm{ac}}\cos(\omega t + \varphi)$ and $\Phi^{(\pm)}(t) = \frac{1}{8}(A \pm 2\Delta_{\varepsilon_z}) - \frac{1}{2}\varepsilon_{\mathrm{ac}}\cos(\omega t + \varphi)$. Let $\delta\varepsilon$ be the smallest difference between diagonal energy levels from different diagonal blocks in $\tilde{H}^{(\mathrm{ac})}$. Then, given that the nonoscillating elements and

the oscillating amplitude $\varepsilon_{\rm ac}$ in the off-diagonal blocks of the Hamiltonian Eq. (11) are smaller than $\delta\varepsilon$, we can use the time-dependent SW (TDSW) transformation to find an analytical effective Hamiltonian in the qubit space. However, as further explained in Appendix A, the driving frequency at resonance is comparable in magnitude to the dominant energy scales in the Hamiltonian and, as a result, a system of differential equations must be solved to find the transformation matrix [42]. This is in contrast to other approaches found in the literature [43,44], where the transformation matrix is found by solving a system of algebraic equations.

Given that the coupling between the orbital ground and excited eigenstates is only non-negligible near the ionization point where $\theta \approx \pi/2$, in the TDSW transformation we neglect the Hamiltonian elements $\propto \cos\theta$. Moreover, the general solution to the system of differential equations that gives the TDSW transformation matrix $e^{S(t)}$ also contains terms $\propto e^{i\varepsilon_0 t}$, whose prefactors are set to zero owing to the requirement that $S(t)$ should be time independent in the absence of oscillating driving ($\varepsilon_{\rm ac} = 0$). The effective ac-driven Hamiltonian in the qubit space is, therefore, given by

$$\begin{aligned} H_{\rm ff}^{\rm (ac)} = \frac{1}{2}\sum_{j=1}^{3}[&(\Omega_{x,0} + \Omega_{x,j}\cos^j(\omega t+\varphi))\sigma_x \\ &- (\Omega_{y,j-1}\cos^{j-1}(\omega t+\varphi))\sin(\omega t+\varphi)\sigma_y \\ &- (\varepsilon_{{\rm ff},0} + \varepsilon_{{\rm ff},j}\cos^j(\omega t+\varphi))\sigma_z], \end{aligned} \tag{12}$$

where $\Omega_{x,i}$, $\Omega_{y,i}$, and $\varepsilon_{{\rm ff},i}$ are given in Appendix B. We can go a step further and use Floquet perturbation theory [32] to derive the effective Hamiltonian in the rotating frame and obtain analytical expressions for the Rabi frequency and resonance frequency. The Floquet method, in short, transforms a time-dependent Schrödinger equation of a periodically driven finite-dimensional Hamiltonian $\mathcal{H}(t)$ into a time-independent Schrödinger equation of an infinite-dimensional Floquet Hamiltonian $\mathcal{H}_F$ defined by [32,43]

$$\langle\alpha' m'|\mathcal{H}_F|\alpha m\rangle = m\omega\delta_{\alpha'\alpha}\delta_{m'm} + \sum_{n=-\infty}^{\infty}\langle\psi_{\alpha'}|\mathcal{H}^{(n)}|\psi_\alpha\rangle\delta_{m',n+m}, \tag{13}$$

where $|\psi_\alpha\rangle$ with $\alpha = 1,\ldots,d_H$ (d_H is the Hilbert space dimension) is an arbitrary basis of the Hilbert space and $\mathcal{H}^{(n)}$ are the Fourier components of the Hamiltonian, $\mathcal{H}(t) = \sum_{n=-\infty}^{\infty}\mathcal{H}^{(n)}e^{in\omega t}$. In our case, the diagonal elements of the Floquet Hamiltonian H_F, obtained from applying the Floquet transformation to Eq. (12), form degenerate pairs when $\omega = -\varepsilon_{{\rm ff},0} - \varepsilon_{{\rm ff},2}/2$. For each of these pairs, the corresponding subspace is weakly coupled to the other diagonal elements and, therefore, it can be treated perturbatively using a time-independent SW transformation. To first-order, SW perturbation theory gives an effective 2×2 Floquet Hamiltonian,

$$\tilde{H}_F = \frac{1}{2}\begin{pmatrix} -\Delta & \Omega_R e^{-i\varphi} \\ \Omega_R e^{i\varphi} & \Delta \end{pmatrix}, \tag{14}$$

where $\Omega_R = \frac{1}{8}(4\Omega_{x,1} + 3\Omega_{x,3} - 4\Omega_{y,0} - \Omega_{y,2})$ and $\Delta = \frac{1}{2}(2\varepsilon_{{\rm ff},0} + \varepsilon_{{\rm ff},2} + 2\omega)$. If $\Delta = 0$, then the qubit is being driven at resonance and, therefore, the resonance and Rabi frequencies are $\omega_{\rm res} = -\varepsilon_{{\rm ff},0} - \varepsilon_{{\rm ff},2}/2$ and $\Omega_{\rm res} = |\Omega_R|$, respectively. This result is exactly equal to the one obtained by neglecting the diagonal oscillating terms in the Hamiltonian and applying RWA. The effective Floquet Hamiltonian Eq. (14) is, therefore, in a rotating frame defined by $U = \exp(-i\omega t\,\sigma_z)$.

The amplitude of the oscillating field, $E^{\rm ac}$, should not be too large that it leads to leakage to higher states, nor should it be too small that the gate time becomes too long. We want a simple expression that can be used to tune $E^{\rm ac}$ to produce fast high-fidelity x rotations. We can use the the ratio between the energy coupling logical states to higher states and the energy gap between those same states. This ratio should be $\ll 1$ to prevent leakage when using the smooth pulses introduced in the previous section. In the rotating frame, the flip-flop Hamiltonian with ac driving with electric field near or at the ionization point ($\Delta E = 0$) presents small energy gaps between the logical states $|*\rangle\, g\,\widetilde{\uparrow\Downarrow}$ and $|*\rangle\, g\,\widetilde{\downarrow\Uparrow}$ and the higher state $|*\rangle\, e\,\widetilde{\downarrow\Uparrow}$. On one hand, the coupling energy between $|*\rangle\, g\,\widetilde{\uparrow\Downarrow}$ and $|*\rangle\, e\,\widetilde{\downarrow\Uparrow}$ does not depend on $E^{\rm ac}$ and is much smaller than their energy gap, and thus undesired transitions are highly unlikely. On the other hand, the coupling energy between $|*\rangle\, g\,\widetilde{\downarrow\Uparrow}$ and $|*\rangle\, e\,\widetilde{\downarrow\Uparrow}$ does depend on $E^{\rm ac}$ and can lead to leakage. We need analytic expressions for the $E^{\rm ac}$-dependent coupling energy and the energy gap between $|*\rangle\, g\,\widetilde{\downarrow\Uparrow}$ and $|*\rangle\, e\,\widetilde{\downarrow\Uparrow}$. We can get those analytic expressions using $\tilde{H}^{\rm (ac)}$ Eq. (11) in the rotating frame with the approximation $\omega_{\rm res} \approx \varepsilon_{\rm ff}$. We use this approximation since the effective flip-flop transition energy $\varepsilon_{\rm ff}$ Eq. (7) is, by far, the dominant term in $\omega_{\rm res}$ and, in contrast to the Rabi frequency, the correcting terms for the resonance frequency obtained with TDSW and Floquet theory are much smaller than $\varepsilon_{\rm ff}$. After some simplifications, we find the following expression for the ratio between the $|*\rangle\, g\,\widetilde{\downarrow\Uparrow} - |*\rangle\, e\,\widetilde{\downarrow\Uparrow}$ coupling energy and energy gap:

$$\frac{\varepsilon_{\rm ac}\sin(\theta)}{4(\varepsilon_0 - \varepsilon_{\rm ff})} = R, \tag{15}$$

where we set the ratio equal to R with $0 < R < 0.5$. Depending on the system parameters, one can try different values for R and use Eq. (15) to find the value for $E^{\rm ac}$ that would produce fast high-fidelity x rotations.

We find it convenient to use the same parameters $\{\varsigma = 1000, \varsigma_{\rm ac} = 2, t_r = 1, R = 0.23\}$ in all the calculations for x rotations presented in Figs. 5(a)–5(c) and Appendix C. The large value for ς suitably decreases the dc pulse slope in the region between the pulse inflection points and plateau of the control pulses, $\Delta E(t)$ and $E^{\rm (ac)}(t)$,that produce the desired x rotation ($\varphi = 0$). Hereafter, all the parameters for the ac pulse ($E^{\rm (ac)}$) are labeled (ac). For the dc pulse, we use the same idle point that was used in the previous section $\Delta E_{\rm idle} = 60\ {\rm kV\ m^{-1}}$. The ac pulse always starts at $E^{\rm (ac)}(t=0) = 0\ {\rm kV\ m^{-1}}$ with a ramp time given by $t_r^{\rm (ac)} = (T - 2t_r)/\rho$ with $\rho = 2.1$, which ensures that the drive amplitude $E^{\rm ac}$ is nonzero only when the electron is at the operating point. We use Eq. (15), the analytical expressions for the resonance $\omega_{\rm res} \approx \varepsilon_{\rm ff}$ and Rabi $\Omega_{\rm res}$ frequencies, and the objective

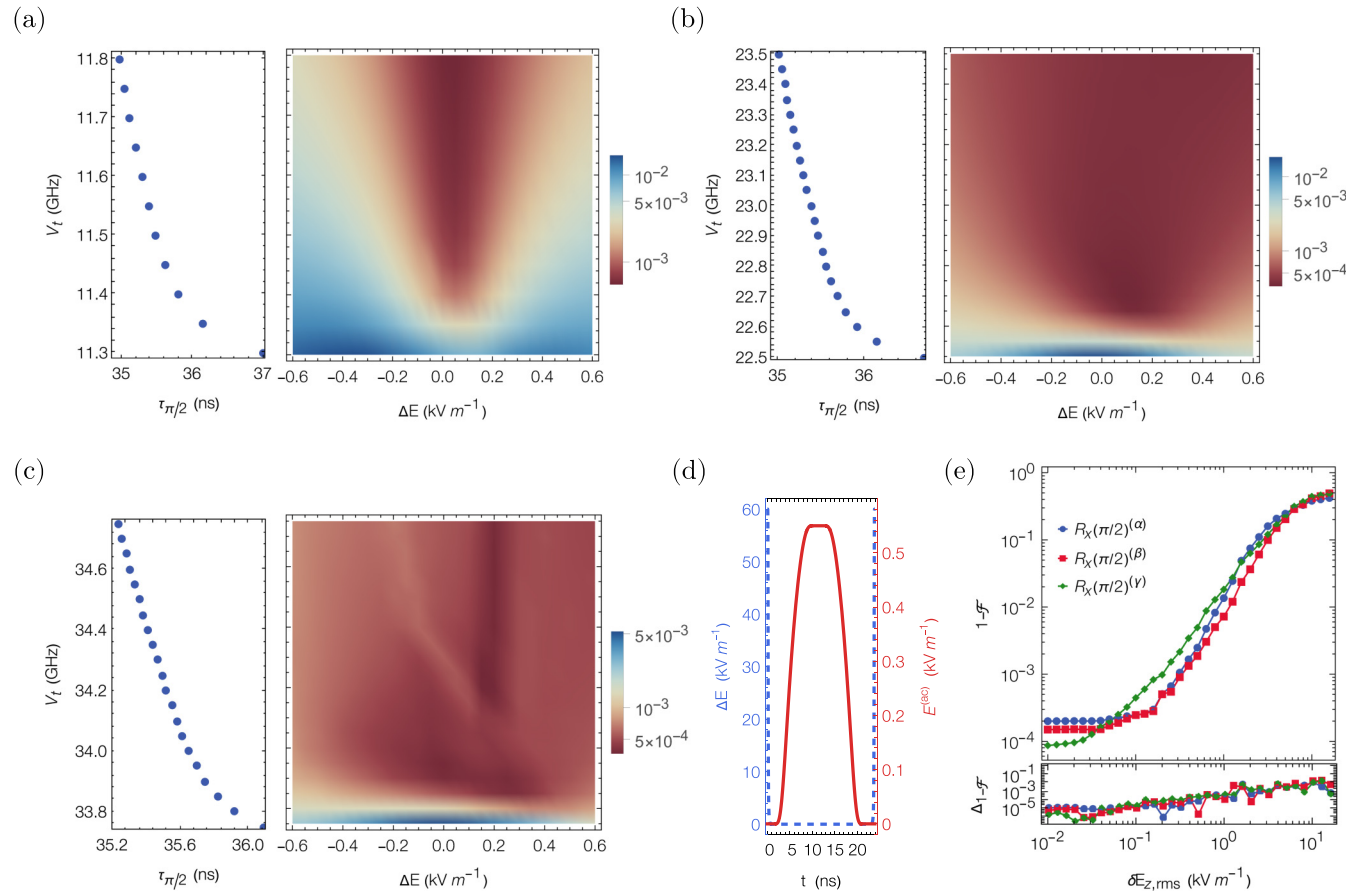

FIG. 5. Infidelity maps and average gate times of $R_x(\pi/2)$ gates for different magnetic field strengths: (a) $B_0 = 0.4$ T, (b) $B_0 = 0.8$ T, (c) $B_0 = 1.2$ T. The pulse operating point (tunnel coupling) is on the horizontal (vertical) axis of each infidelity map. We use two pulses, given by Eq. (6), one for the dc component [dashed blue curve in (d)] of the electric field and one for the ac component [solid red curve in (d)], the pulse parameters corresponding to the latter are labeled (ac). All dc (ac) pulses start at $\xi_0 = 60$ kV m^{-1}($\xi_0^{(\mathrm{ac})} = 0$ kV m^{-1}) and have $\varsigma = 1000$ and $t_r = 1$. The ac ramp time is given by $t_r^{(\mathrm{ac})} = (T - 2t_r)/\rho$, with $\rho = 2.1$ being a scale factor, and all ac pulses have $\varsigma_{\mathrm{ac}} = 2$. Each point in the fidelity map is the result of averaging 100 samples taken from a uniformly distributed noise in the range $\sqrt{3}[-\delta E_{z,\mathrm{rms}}, \delta E_{z,\mathrm{rms}}]$ with $\delta E_{z,\mathrm{rms}} = 100$ V m^{-1}. For the ac pulse, $\xi_f^{(\mathrm{ac})}$ is easily obtained by solving Eq. (15) with $R = 0.23$. The plots to the left of each infidelity map depict the average gate time (horizontal axis) under different values of the tunnel coupling (vertical axis). (d) Electric field dc amplitude ΔE (dashed blue curve) and ac amplitude $E^{(\mathrm{ac})}$ (solid red curve) pulse shapes used to implement $R_x(\pi/2)^{(\alpha)}$ in (e). (e) Upper part: Infidelity of $\pi/2$ x rotations as a function of various electric field noise strength values $\delta E_{z,\mathrm{rms}}$ and fixed tunnel coupling noise $\delta V_{t,\mathrm{rms}}$. The tunnel coupling noise and pulse parameters for each gate are given in Table II. Lower part: Change in infidelity $\Delta_{1-\mathcal{F}}$ between gate infidelity calculated with only electric field noise δE_z and gate infidelity calculated with noise on both electric field δE_z and tunnel coupling δV_t.

function

$$\Theta(T) = \left| \mathrm{mod}\left[\int_{t_r}^{T-t_r} \Omega_{\mathrm{res}}(t)dt, 2\pi \right] - \phi \right| \qquad (16)$$

to find the corresponding gate time T. Here, ϕ is the target rotation angle, and mod is the modulo operation. This procedure gives a full set of parameters which produces high-fidelity x rotations with the ac Hamiltonian in the dc eigenbasis.

Figures 5(a)–5(c) show the infidelity maps for $\pi/2$ x rotations for three different magnetic field strengths (0.4 T, 0.8 T, 1.2 T) commonly used in the laboratory and average gate times corresponding to different tunnel coupling values. The infidelities are averaged over the strength of a quasistatic noise by sampling a random perturbation δE_z, which is linearly added to $\Delta E(t)$, over a uniform distribution in the range $\sqrt{3}[-\delta E_{z,\mathrm{rms}}, \delta E_{z,\mathrm{rms}}]$ with $\delta E_{z,\mathrm{rms}} = 100$ Vm^{-1}. In Figs. 5(a)–5(c) we see that with an external magnetic field of (i) 0.4 T (ii) 0.8 T (*iii*) 1.2 T and $\Delta E = 0$, a V_t less than (i) 11.35 GHz, (ii) 22.55 GHz, (iii) 33.8 GHz leads to an average fidelity less than (i) 99.4%, (ii) 98.9%, (iii) 99.7% for noise level $\delta E_{z,\mathrm{rms}} = 100$ Vm^{-1}. In the upper part of Fig. 5(e), we present the gate infidelities of three $\pi/2$ x rotations, each with different magnetic field strength, for different strengths of the electric field noise $\delta E_{z,\mathrm{rms}}$ and a fixed tunnel coupling noise amplitude $\delta V_{t,\mathrm{rms}}$. The system and pulse parameters for these three gates are given in Table II. The control pulse shapes for $\Delta E(t)$ and $E^{(\mathrm{ac})}(t)$ that are used to implement $R_x(\pi/2)^{(\alpha)}$ in Fig. 5(e) are shown in Fig. 5(d). In contrast to the infidelity maps in Figs. 5(a)–5(c), the average gate infidelity in Fig. 5(e) is obtained by sampling random perturbations δE_z and δV_t over uniform distributions with range $\sqrt{3}[-\delta E_{z,\mathrm{rms}}, \delta E_{z,\mathrm{rms}}]$ and $\sqrt{3}[-\delta V_{t,\mathrm{rms}}, \delta V_{t,\mathrm{rms}}]$, respectively. The infidelity average

TABLE II. System and pulse parameters for each infidelity curve in Fig. 5(e). For each curve, the stated average gate fidelity $\mathcal{F}$ is calculated assuming electric field noise $\delta E_{z,\mathrm{rms}} = 100$ V m^{-1} and tunnel coupling noise $\delta V_{t,\mathrm{rms}}$ indicated in this table. The ac ramp time is the same for each gate and is given by $t_r^{(\mathrm{ac})} = (T - 2t_r)/2.1$.

	$R_x(\pi/2)^{(\alpha)}$	$R_x(\pi/2)^{(\beta)}$	$R_x(\pi/2)^{(\gamma)}$
B_0 (T)	0.4	0.8	1.2
$V_t/2\pi$ (GHz)	12.5	24.5	34.5
ΔE_{op} (kVm^{-1})	0	0	1.5
t_r	1	1	1
ς	1000	1000	1000
$\varsigma^{(\mathrm{ac})}$	2	2	2
R	0.38	0.4	0.4
$E^{(\mathrm{ac})}$ (kVm^{-1})	0.55	0.94	0.62
$\delta V_{t,\mathrm{rms}}/2\pi$ (MHz)	2.9	3.3	3.5
T (ns)	23.86	23.42	24.23
$\mathcal{F}$ (%)	99.98	99.98	99.96

is taken over 200 samples for each value of $\delta E_{z,\mathrm{rms}}$, and the same amount of samples for the value of $\delta V_{t,\mathrm{rms}}$ given in Table II. The lower part of Fig. 5(e) shows the change in infidelity $\Delta_{1-\mathcal{F}}$ that happens when only electric field noise is taken into account. Similarly to the z rotation case in Sec. III, $\Delta_{1-\mathcal{F}}$ shows that including tunnel coupling noise in the gate infidelity calculation produces a change that is at least an order of magnitude lower than the infidelity value obtained with only electric field noise. Lastly, for each x rotation in Fig. 5(e), we find that shifts in the control pulse length of less than ± 1 ns can at most reduce the gate fidelity by an order of magnitude (see Appendix E for further details).

The numerical results presented in Fig. 5 show that our pulses can easily generate fast high-fidelity x rotation for any magnetic field strength and a wide combination of tunnel coupling energies and electric field values. Moreover, in Appendix C we present an extended version of the maps presented in Fig. 5, which show that fast high-fidelity x rotation can be implemented with large tunnel coupling energies and electric fields not necessarily close to the ionization point. The use of large tunnel coupling energies can also increase the relaxation time by a few orders of magnitude, even more if the best operating point is not near the ionization point like it is in the case with $B_0 = 1.2$ T and $V_t > 34$ GHz [see Fig. 6(c)].

V. CONCLUSIONS

We have presented control schemes to produce fast high-fidelity z and x rotations for flip-flop qubits in silicon. Using both time-independent and TDSW transformations and Floquet perturbation theories, we derived analytical expressions for the effective qubit Hamiltonian in the presence or absence of periodic driving. With these analytical expressions, we numerically optimized the parameters of a modified Planck-taper window function such that it implements high-fidelity single-qubit gates in the shortest possible time. We proposed

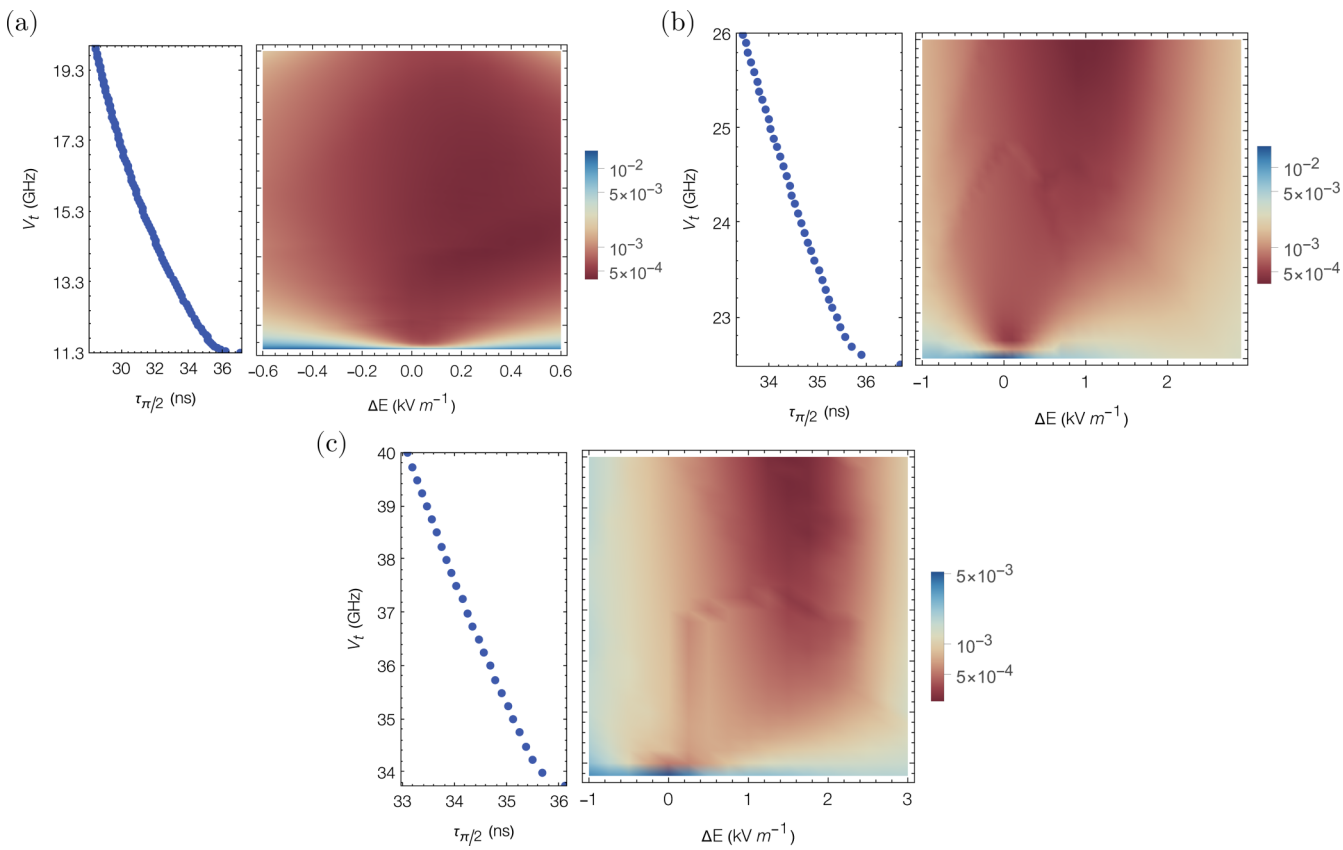

FIG. 6. Extended infidelity maps and average gate times corresponding to the maps in Fig. 5 of the main text.

fast z and x rotations with fidelities around 99.99% in the presence of realistic noise levels of 0.1 kV m^{-1}, and gate times much shorter than previously reported. Moreover, since our method does not rely on sweet spots (clock transitions), we presented fast high-fidelity single-qubit gates with magnetic fields stronger than what was previously proposed and closer to what is commonly used in the laboratory. Finally, the flexibility of our method allows the implementation of single-qubit gates with relaxation times and qubit quality factors five (one) orders of magnitude larger than those corresponding to clock-transition-based z rotations (x rotations).

ACKNOWLEDGMENTS

We thank A. Morello for helpful discussions. This work is supported by the Army Research Office (No. W911NF-17-0287).

APPENDIX A: TIME-DEPENDENT SCHRIEFFER-WOLFF PERTURBATION THEORY

Before introducing the TDSW perturbation theory, we briefly review the time-independent version of it [31,45].

Let us consider a general Hamiltonian $\mathcal{H} = \mathcal{H}_0 + \mathcal{H}'$, where $\mathcal{H}_0$ is purely diagonal and $\mathcal{H}' = \mathcal{H}_1 + \mathcal{H}_2$ is the perturbation. Assuming that the basis states of $\mathcal{H}$ are divided into two weakly interacting, energetically well-separated subspaces (diagonal blocks), then $\mathcal{H}_1$ is block diagonal with zeros as diagonal elements and $\mathcal{H}_2$ is strictly block-off-diagonal. The SW transformation aims to decouple these two subspaces, transforming $\mathcal{H}$ into a block-diagonal Hamiltonian $\tilde{\mathcal{H}}$. In principle, $\tilde{\mathcal{H}}$ can be obtained via a unitary transformation: $\tilde{\mathcal{H}} = e^{-S}\mathcal{H}e^{S}$, where S is a block-off-diagonal anti-Hermitian operator. In most of the cases, however, S is not known and must be constructed. This is done by first substituting e^{S} in the unitary transformation with its series expansion, obtaining

$$\tilde{\mathcal{H}} = \sum_{j=0}^{\infty} \frac{1}{j!}[\mathcal{H}_0 + \mathcal{H}_1, S]_{(j)} + \sum_{j=0}^{\infty} \frac{1}{j!}[\mathcal{H}_2, S]_{(j)}, \tag{A1}$$

with $[\mathcal{H}, S]_{(m+1)} = [[\mathcal{H}, S]_{(m)}, S]$ and $[\mathcal{H}, S]_{(0)} = \mathcal{H}$. Since the block-off-diagonal unitary transformation e^{S} must be close to unity due to the weakly interacting subspaces, then S is small and can be expanded as a power series in the perturbation. Finally, each order of S is determined successively by setting the block-off-diagonal part of $\tilde{\mathcal{H}}$ equal to zero and solving it order by order.

In TDSW, the block-off-diagonal anti-Hermitian operator S is time dependent and, therefore, the unitary transformation that, in principle, can be used to obtain $\tilde{\mathcal{H}}(t)$ is now given by

$$\tilde{\mathcal{H}}(t) = e^{-S(t)}\mathcal{H}(t)e^{S(t)} + i\frac{\partial e^{-S(t)}}{\partial t}e^{S(t)}. \tag{A2}$$

A time-dependent version of Eq. (A1) is obtained by plugging the series expansion of e^{S} into Eq. (A2),

$$\begin{aligned}\tilde{\mathcal{H}} = &\sum_{j=0}^{\infty} \frac{1}{j!}[\mathcal{H}_0 + \mathcal{H}_1, S]_{(j)} + \sum_{j=0}^{\infty} \frac{1}{j!}[\mathcal{H}_2, S]_{(j)} \\ &- i\sum_{j=0}^{\infty} \frac{1}{(j+1)!}[\dot{S}, S]_{(j)},\end{aligned} \tag{A3}$$

where $\dot{S}(t) = \partial_t S(t)$. Given that $S(t)$ is block-off-diagonal, the block-diagonal part $\tilde{\mathcal{H}}_{\text{diag}}$ of $\tilde{\mathcal{H}}$ contains the terms $[\mathcal{H}_0 + \mathcal{H}_1, S]_{(j)}$ with even j and the terms $[\mathcal{H}_2, S]_{(j)}$ and $[\dot{S}, S]_{(j)}$ with odd j. The same goes for the block-off-diagonal part $\tilde{\mathcal{H}}_{\text{off}}$ but with odd j instead of even j and vice versa:

$$\begin{aligned}\tilde{\mathcal{H}}_{\text{off}} = &\sum_{j=0}^{\infty} \frac{1}{(2j+1)!}[\mathcal{H}_0 + \mathcal{H}_1, S]_{(2j+1)} \\ &+ \sum_{j=0}^{\infty} \frac{1}{(2j)!}[\mathcal{H}_2, S]_{(2j)} \\ &- i\sum_{j=0}^{\infty} \frac{1}{(2j+1)!}[\dot{S}, S]_{(2j)},\end{aligned} \tag{A4}$$

$$\begin{aligned}\tilde{\mathcal{H}}_{\text{diag}} = &\sum_{j=0}^{\infty} \frac{1}{(2j)!}[\mathcal{H}_0 + \mathcal{H}_1, S]_{(2j)} \\ &+ \sum_{j=0}^{\infty} \frac{1}{(2j+1)!}[\mathcal{H}_2, S]_{(2j+1)} \\ &- i\sum_{j=0}^{\infty} \frac{1}{(2j+2)!}[\dot{S}, S]_{(2j+1)}.\end{aligned} \tag{A5}$$

The expansion of $S = \sum_j S_j$ as a power series in the perturbation permits to solve $\tilde{\mathcal{H}}_{\text{off}} = 0$ order by order. Here, S_j is of jth order in the perturbation. It is not immediately obvious, however, what order $\dot{S}_j$ is. Since the driving frequency ω is expected to characterize the time evolution of S_j, then we can assume that $\dot{S}_j \sim \omega S_j$ [43]. Now, in the particular case of the flip-flop qubit, for most values of ΔE the driving frequency ω, the spin energy splitting ε_s, the hyperfine interaction A, and the driving amplitude energy ε_{ac} are much smaller than the orbital splitting ε_0. However, around the ionization point, where the fastest $x(y)$ gates are obtained, $\omega \sim \varepsilon_s \sim \varepsilon_0$ and, therefore, ω cannot be treated as a perturbation. As a result, $\dot{S}_j$ and S_j are both of jth order in the perturbation.

The order-by-order expansion of $\tilde{\mathcal{H}}_{\text{off}} = 0$ gives a differential equation for each S_j matrix operator. The first few equations are

$$\begin{aligned}[\mathcal{H}_0, S_1] &= -\mathcal{H}_2 + i\dot{S}_1, \\ [\mathcal{H}_0, S_2] &= -[\mathcal{H}_1, S_1] + i\dot{S}_2, \\ [\mathcal{H}_0, S_3] &= -[\mathcal{H}_1, S_2] - \tfrac{1}{3}[\mathcal{H}_2, S_1]_{(2)} + i\dot{S}_3.\end{aligned} \tag{A6}$$

These equations, apart from determining the operator $S(t)$ in the transformation, can also be used to simplify Eq. (A5). The first few terms, then, that form the effective block-diagonal Hamiltonian $\tilde{\mathcal{H}} = \sum_j \tilde{\mathcal{H}}_j$ are

$$\begin{aligned}\tilde{\mathcal{H}}_0 &= \mathcal{H}_0, \\ \tilde{\mathcal{H}}_1 &= \mathcal{H}_1, \\ \tilde{\mathcal{H}}_2 &= \tfrac{1}{2}[\mathcal{H}_2, S_1], \\ \tilde{\mathcal{H}}_3 &= \tfrac{1}{2}[\mathcal{H}_2, S_2], \\ \tilde{\mathcal{H}}_4 &= \tfrac{1}{2}[\mathcal{H}_2, S_3] - \tfrac{1}{4}[\mathcal{H}_2, S_1]_{(3)}.\end{aligned} \tag{A7}$$

APPENDIX B: ANALYTICAL EXPRESSIONS FOR THE ELEMENTS OF THE AC-DRIVEN HAMILTONIAN

The elements of the ac-driven Hamiltonian Eq. (12) in the main text have the following form:

$$\Omega_{x,0} = \frac{A\sin^2\theta}{8\left(\varepsilon_0^2-\varepsilon_{s^{(-)}}^2\right)}\left(-\Delta_{\varepsilon_z}\varepsilon_{s^{(-)}} + \frac{A\left(2\varepsilon_0^2-\varepsilon_{s^{(-)}}^2\right)}{2\varepsilon_0} - \frac{A^2\varepsilon_0^2(5A\varepsilon_0 - 8\Delta_{\varepsilon_z}\varepsilon_{s^{(-)}})\sin^2\theta}{32\left(\varepsilon_0^2-\varepsilon_{s^{(-)}}^2\right)^2}\right) + \frac{A\varepsilon_{\rm ac}^2\sin^4\theta}{64\left(\varepsilon_0^2-\varepsilon_{s^{(-)}}^2\right)^3}\left(\Delta_{\varepsilon_z}\varepsilon_{s^{(-)}}\left(9\varepsilon_0^2-\varepsilon_{s^{(-)}}^2\right) - \frac{A\left(91\varepsilon_0^4-126\varepsilon_0^2\varepsilon_{s^{(-)}}^2+51\varepsilon_{s^{(-)}}^4\right)}{16\varepsilon_0}\right),$$

$$\Omega_{x,1} = -\frac{A\varepsilon_0\varepsilon_{\rm ac}\sin^2\theta}{2\left(\varepsilon_0^2-\varepsilon_{s^{(-)}}^2\right)} + \frac{A\varepsilon_{\rm ac}\sin^4\theta}{128\varepsilon_0\left(\varepsilon_0^2-\varepsilon_{s^{(-)}}^2\right)^3} \times \left(A^2\left(10\varepsilon_0^2-\varepsilon_{s^{(-)}}^2\right)\left(\varepsilon_0^2+\varepsilon_{s^{(-)}}^2\right) + \varepsilon_{\rm ac}^2\left(27\varepsilon_0^4-14\varepsilon_0^2\varepsilon_{s^{(-)}}^2+3\varepsilon_{s^{(-)}}^4\right)\right),$$

$$\Omega_{x,2} = \frac{A\varepsilon_{\rm ac}^2\sin^4\theta}{32\left(\varepsilon_0^2-\varepsilon_{s^{(-)}}^2\right)^3}\left(-\Delta_{\varepsilon_z}\varepsilon_{s^{(-)}}\left(5\varepsilon_0^2-2\varepsilon_{s^{(-)}}^2\right) + \frac{A\left(59\varepsilon_0^4-102\varepsilon_0^2\varepsilon_{s^{(-)}}^2+27\varepsilon_{s^{(-)}}^4\right)}{16\varepsilon_0}\right),$$

$$\Omega_{x,3} = -\frac{A\varepsilon_{\rm ac}^3\sin^4\theta\left(13\varepsilon_0^4-34\varepsilon_0^2\varepsilon_{s^{(-)}}^2+5\varepsilon_{s^{(-)}}^4\right)}{128\varepsilon_0\left(\varepsilon_0^2-\varepsilon_{s^{(-)}}^2\right)^3},$$

$$\Omega_{y,0} = \frac{A^2\varepsilon_{\rm ac}\sin^4\theta}{128\left(\varepsilon_0^2-\varepsilon_{s^{(-)}}^2\right)^2}\left(-9\Delta_{\varepsilon_z}\varepsilon_{s^{(-)}} + \frac{A\left(4\varepsilon_0^4-9\varepsilon_0^2\varepsilon_{s^{(-)}}^2+3\varepsilon_{s^{(-)}}^4\right)}{\varepsilon_0\left(\varepsilon_0^2-\varepsilon_{s^{(-)}}^2\right)}\right),$$

$$\Omega_{y,1} = \frac{A\varepsilon_{\rm ac}^2\sin^4\theta}{32\left(\varepsilon_0^2-\varepsilon_{s^{(-)}}^2\right)^3}\left(-3\Delta_{\varepsilon_z}\varepsilon_0^2\varepsilon_{s^{(-)}} - \frac{A\left(91\varepsilon_0^4-126\varepsilon_0^2\varepsilon_{s^{(-)}}^2+51\varepsilon_{s^{(-)}}^4\right)}{16\varepsilon_0}\right),$$

$$\Omega_{y,2} = \frac{A\varepsilon_{\rm ac}^3\sin^4\theta\left(27\varepsilon_0^4-14\varepsilon_0^2\varepsilon_{s^{(-)}}^2+3\varepsilon_{s^{(-)}}^4\right)}{128\varepsilon_0\left(\varepsilon_0^2-\varepsilon_{s^{(-)}}^2\right)^3},$$

$$\varepsilon_{\rm ff,0} = \varepsilon_{\rm ff} + \frac{A\varepsilon_{\rm ac}^2\sin^4\theta}{64\left(\varepsilon_0^2-\varepsilon_{s^{(-)}}^2\right)^2}\left(\frac{\Delta_{\varepsilon_z}\left(\varepsilon_0^2+\varepsilon_{s^{(-)}}^2\right)}{\varepsilon_0} + \frac{A\varepsilon_{s^{(-)}}\left(9\varepsilon_0^2-\varepsilon_{s^{(-)}}^2\right)}{\varepsilon_0^2-\varepsilon_{s^{(-)}}^2}\right),$$

$$\varepsilon_{\rm ff,1} = \frac{\Delta_{\varepsilon_z}\varepsilon_{\rm ac}\left(2\varepsilon_0^2-\varepsilon_{s^{(-)}}^2\right)\sin^2\theta}{4\varepsilon_0\left(\varepsilon_0^2-\varepsilon_{s^{(-)}}^2\right)} + \frac{A^3\varepsilon_{\rm ac}\sin^4\theta\left(4\varepsilon_0^2\varepsilon_{s^{(-)}}-3\varepsilon_{s^{(-)}}^3\right)}{128\left(\varepsilon_0^2-\varepsilon_{s^{(-)}}^2\right)^3} - \frac{\Delta_{\varepsilon_z}\varepsilon_{\rm ac}\sin^4\theta}{256\varepsilon_0\left(\varepsilon_0^2-\varepsilon_{s^{(-)}}^2\right)^3} \times \left(\varepsilon_{\rm ac}^2\left(91\varepsilon_0^4-126\varepsilon_0^2\varepsilon_{s^{(-)}}^2+51\varepsilon_{s^{(-)}}^4\right) + A^2\left(28\varepsilon_0^4-11\varepsilon_0^2\varepsilon_{s^{(-)}}^2+6\varepsilon_{s^{(-)}}^4-\frac{3\varepsilon_{s^{(-)}}^6}{\varepsilon_0^2}\right)\right),$$

$$\varepsilon_{\rm ff,2} = \frac{A\varepsilon_{\rm ac}^2\sin^4\theta}{16\left(\varepsilon_0^2-\varepsilon_{s^{(-)}}^2\right)^2}\left(-\frac{A\varepsilon_{s^{(-)}}\left(5\varepsilon_0^2-\varepsilon_{s^{(-)}}^2\right)}{2\left(\varepsilon_0^2-\varepsilon_{s^{(-)}}^2\right)} - \frac{\Delta_{\varepsilon_z}\left(\varepsilon_0^2-2\varepsilon_{s^{(-)}}^2\right)}{\varepsilon_0}\right),$$

$$\varepsilon_{\rm ff,3} = \frac{\Delta_{\varepsilon_z}\varepsilon_{\rm ac}^3\sin^4\theta\left(25\varepsilon_0^2-13\varepsilon_{s^{(-)}}^2\right)}{64\varepsilon_0\left(\varepsilon_0^2-\varepsilon_{s^{(-)}}^2\right)^2}.$$

APPENDIX C: EXTENDED INFIDELITY MAPS

Figure 6 shows extended versions of the infidelity maps and gate times for $\pi/2$ x rotations shown in Figs. 5(a)–5(c) of the main text.

APPENDIX D: GATE INFIDELITY FOR Z ROTATIONS WITH WEAKER TUNNEL COUPLINGS

We show in Fig. 7 gate infidelities and gate times for the same z rotations from Fig. 4(b) in the main text. We calculate the gate infidelities and gate times using lower tunnel coupling values than those used in the main text. The gate infidelity is the result of averaging 100 samples for δE_z taken from a uniform distribution in the range $\sqrt{3}[-\delta E_{z,\rm rms}, \delta E_{z,\rm rms}]$ with $\delta E_{z,\rm rms} = 100$ Vm^{-1}. These results show that using an operating point $\Delta E_{\rm op}$ closer to the donor instead of near to the ionization point generates fast high-fidelity z rotations even for tunnel coupling values of a few GHz.

APPENDIX E: GATE INFIDELITY SENSITIVITY TO PULSE LENGTH PERTURBATION

Here we show the effect of pulse overshoot/undershoot on the infidelities of the gates presented in the main text. The gate infidelities shown in Fig. 8 were obtained with the same system and pulse parameters of the z rotations and x rotations given by Tables I and II in the main text. In each case, to calculate the gate infidelity, we average 100 sampled for δE_z (electric field noise) taken from a uniform distribution in the range $\sqrt{3}[-\delta E_{z,\rm rms}, \delta E_{z,\rm rms}]$ with $\delta E_{z,\rm rms} = 100$ Vm^{-1}. For z rotations, variations in the pulse length of ± 1 ns can lead to an infidelity increase between one and three orders of magnitude. For x rotations, on the other hand, variations in the pulse length of ± 2 ns can lead to an infidelity increase of approximately one order of magnitude.

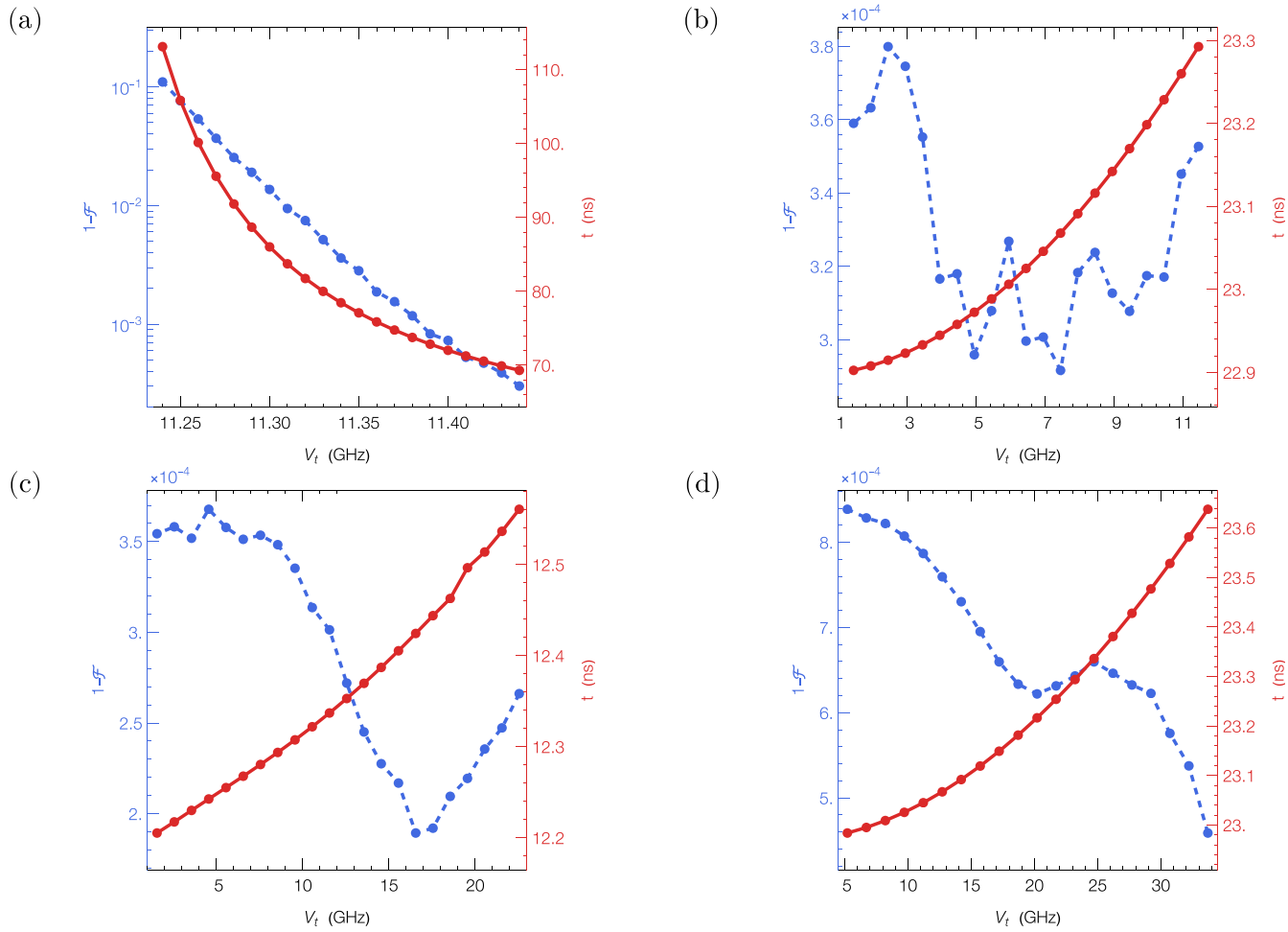

FIG. 7. Gate infidelities and gate times for the z-rotations (a) $R_z(\pi)^{(\alpha)}$, (b) $R_z(\pi)^{(\beta)}$, (c) $R_z(\pi)^{(\gamma)}$, (d) $R_z(\pi)^{(\delta)}$, presented in Fig. 4(b). We use the same system and pulse parameters, except for the tunnel coupling, given in Table I.

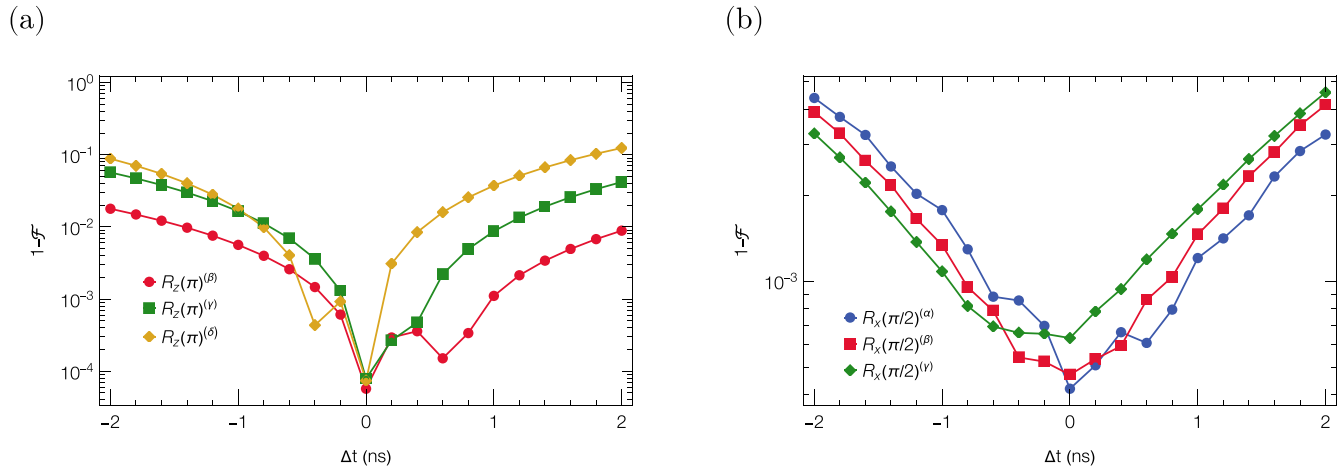

FIG. 8. Gate infidelities for (a) z rotations presented in Fig. 4(b) and (b) x rotations presented in Fig. 5(e), obtained after perturbing their respective gate times by Δt.

[1] M. A. Nielsen and I. L. Chuang, *Quantum Computation and Quantum Information* (Cambridge University Press, Cambridge, 2010).

[2] K. M. Itoh and H. Watanabe, Isotope engineering of silicon and diamond for quantum computing and sensing applications, MRS Commun. **4**, 143 (2014).

[3] W. M. Witzel, M. S. Carroll, A. Morello, Ł. Cywiński, and S. Das Sarma, Electron Spin Decoherence in Isotope-Enriched Silicon, Phys. Rev. Lett. **105**, 187602 (2010).

[4] A. M. Tyryshkin, S. Tojo, J. J. L. Morton, H. Riemann, N. V. Abrosimov, P. Becker, H.-j. Pohl, T. Schenkel, M. L. W. Thewalt, K. M. Itoh, and S. A. Lyon, Electron spin coherence exceeding seconds in high-purity silicon, Nat. Mater. **11**, 143 (2012).

[5] F. A. Zwanenburg, A. S. Dzurak, A. Morello, M. Y. Simmons, L. C. L. Hollenberg, G. Klimeck, S. Rogge, S. N. Coppersmith, and M. A. Eriksson, Silicon quantum electronics, Rev. Mod. Phys. **85**, 961 (2013).

[6] P. Harvey-Collard, N. T. Jacobson, M. Rudolph, J. Dominguez, G. A. Ten Eyck, J. R. Wendt, T. Pluym, J. K. Gamble, M. P. Lilly, M. Pioro-Ladrière, and M. S. Carroll, Coherent coupling between a quantum dot and a donor in silicon, Nat. Commun. **8**, 1029 (2017).

[7] A. Chatterjee, P. Stevenson, S. De Franceschi, A. Morello, N. de Leon, and F. Kuemmeth, Semiconductor qubits in practice, Nat. Rev. Phys. **3**, 157 (2021).

[8] T. Struck, A. Hollmann, F. Schauer, O. Fedorets, A. Schmidbauer, K. Sawano, H. Riemann, N. V. Abrosimov, Ł. Cywiński, D. Bougeard, and L. R. Schreiber, Low-frequency spin qubit energy splitting noise in highly purified ^{28}Si/SiGe, npj Quantum Inf. **6**, 40 (2020).

[9] A. Morello, J. J. Pla, P. Bertet, and D. N. Jamieson, Donor spins in silicon for quantum technologies, Adv. Quantum Technol. **3**, 2000005 (2020).

[10] J. T. Muhonen, J. P. Dehollain, A. Laucht, F. E. Hudson, R. Kalra, T. Sekiguchi, K. M. Itoh, D. N. Jamieson, J. C. McCallum, A. S. Dzurak, and A. Morello, Storing quantum information for 30 seconds in a nanoelectronic device, Nat. Nanotechnol. **9**, 986 (2014).

[11] S. B. Tenberg, S. Asaad, M. T. Mądzik, M. A. I. Johnson, B. Joecker, A. Laucht, F. E. Hudson, K. M. Itoh, A. M. Jakob, B. C. Johnson, D. N. Jamieson, J. C. McCallum, A. S. Dzurak, R. Joynt, and A. Morello, Electron spin relaxation of single phosphorus donors in metal-oxide-semiconductor nanoscale devices, Phys. Rev. B **99**, 205306 (2019).

[12] K. Saeedi, S. Simmons, J. Z. Salvail, P. Dluhy, H. Riemann, N. V. Abrosimov, P. Becker, H.-J. Pohl, J. J. L. Morton, and M. L. W. Thewalt, Room-temperature quantum bit storage exceeding 39 minutes using ionized donors in silicon-28, Science **342**, 830 (2013).

[13] J. J. Pla, K. Y. Tan, J. P. Dehollain, W. H. Lim, J. J. L. Morton, F. A. Zwanenburg, D. N. Jamieson, A. S. Dzurak, and A. Morello, High-fidelity readout and control of a nuclear spin qubit in silicon, Nature (London) **496**, 334 (2013).

[14] J. T. Muhonen, A. Laucht, S. Simmons, J. P. Dehollain, R. Kalra, F. E. Hudson, S. Freer, K. M. Itoh, D. N. Jamieson, J. C. McCallum, A. S. Dzurak, and A. Morello, Quantifying the quantum gate fidelity of single-atom spin qubits in silicon by randomized benchmarking, J. Phys.: Condens. Matter **27**, 154205 (2015).

[15] J. T. Muhonen, J. P. Dehollain, A. Laucht, S. Simmons, R. Kalra, F. E. Hudson, A. S. Dzurak, A. Morello D. N. Jamieson, J. C. McCallum, and K. M. Itoh, Coherent control via weak measurements in ^{31}P single-atom electron and nuclear spin qubits, Phys. Rev. B **98**, 155201 (2018).

[16] B. E. Kane, A silicon-based nuclear spin quantum computer, Nature (London) **393**, 133 (1998).

[17] J. P. Dehollain, J. T. Muhonen, K. Y. Tan, A. Saraiva, D. N. Jamieson, A. S. Dzurak, and A. Morello, Single-Shot Readout and Relaxation of Singlet and Triplet States in Exchange-Coupled ^{31}p electron spins in silicon, Phys. Rev. Lett. **112**, 236801 (2014).

[18] Y. Song and S. Das Sarma, Statistical exchange-coupling errors and the practicality of scalable silicon donor qubits, Appl. Phys. Lett. **109**, 253113 (2016).

[19] R. Kalra, A. Laucht, C. D. Hill, and A. Morello, Robust Two-Qubit Gates for Donors in Silicon Controlled by Hyperfine Interactions, Phys. Rev. X **4**, 021044 (2014).

[20] C. D. Hill, E. Peretz, S. J. Hile, M. G. House, M. Fuechsle, S. Rogge, M. Y. Simmons, and L. C. L. Hollenberg, A surface code quantum computer in silicon, Sci. Adv. **1**, e1500707 (2015).

[21] M. T. Mądzik, A. Laucht, F. E. Hudson, A. M. Jakob, B. C. Johnson, D. N. Jamieson, K. M. Itoh, A. S. Dzurak, and A. Morello, Conditional quantum operation of two exchange-coupled single-donor spin qubits in a MOS-compatible silicon device, Nat. Commun. **12**, 181 (2021).

[22] L. Trifunovic, O. Dial, M. Trif, J. R. Wootton, R. Abebe, A. Yacoby, and D. Loss, Long-Distance Spin-Spin Coupling Via Floating Gates, Phys. Rev. X **2**, 011006 (2012).

[23] F. A. Mohiyaddin, R. Kalra, A. Laucht, R. Rahman, G. Klimeck, and A. Morello, Transport of spin qubits with donor chains under realistic experimental conditions, Phys. Rev. B **94**, 045314 (2016).

[24] G. Pica, B. W. Lovett, R. N. Bhatt, T. Schenkel, and S. A. Lyon, Surface code architecture for donors and dots in silicon with imprecise and nonuniform qubit couplings, Phys. Rev. B **93**, 035306 (2016).

[25] G. Tosi, F. A. Mohiyaddin, V. Schmitt, S. Tenberg, R. Rahman, G. Klimeck, and A. Morello, Silicon quantum processor with robust long-distance qubit couplings, Nat. Commun. **8**, 450 (2017).

[26] P. Boross, G. Széchenyi, and A. Pályi, Valley-enhanced fast relaxation of gate-controlled donor qubits in silicon, Nanotechnology **27**, 314002 (2016).

[27] D. Pines, J. Bardeen, and C. P. Slichter, Nuclear polarization and impurity-state spin relaxation processes in silicon, Phys. Rev. **106**, 489 (1957).

[28] A. G. Fowler, M. Mariantoni, J. M. Martinis, and A. N. Cleland, Surface codes: Towards practical large-scale quantum computation, Phys. Rev. A **86**, 032324 (2012).

[29] A. Morello, J. J. Pla, F. A. Zwanenburg, K. W. Chan, K. Y. Tan, H. Huebl, M. Möttönen, C. D. Nugroho, C. Yang, J. A. van Donkelaar, A. D. C. Alves, D. N. Jamieson, C. C. Escott, L. C. L. Hollenberg, R. G. Clark, and A. S. Dzurak, Single-shot readout of an electron spin in silicon, Nature (London) **467**, 687 (2010).

[30] J. P. Dehollain, J. J. Pla, E. Siew, K. Y. Tan, A. S. Dzurak, and A. Morello, Nanoscale broadband transmission lines for spin qubit control, Nanotechnology **24**, 015202 (2013).

[31] J. Schrieffer and P. Wolff, Relation between the Anderson and Kondo Hamiltonians, Phys. Rev. **149**, 491 (1966).

[32] J. H. Shirley, Solution of the Schrödinger equation with a Hamiltonian periodic in time, Phys. Rev. **138**, B979 (1965).

[33] R. Rahman, S. H. Park, T. B. Boykin, G. Klimeck, S. Rogge, and L. C. L. Hollenberg, Gate-induced g-factor control and dimensional transition for donors in multivalley semiconductors, Phys. Rev. B **80**, 155301 (2009).

[34] D. J. A. McKechan, C. Robinson, and B. S. Sathyaprakash, A tapering window for time-domain templates and simulated signals in the detection of gravitational waves from coalescing compact binaries, Classical Quantum Gravity **27**, 084020 (2010).

[35] J. H. Van Vleck, On σ-type doubling and electron spin in the spectra of diatomic molecules, Phys. Rev. **33**, 467 (1929).

[36] I. Shavitt and L. T. Redmon, Quasidegenerate perturbation theories. A canonical van Vleck formalism and its relationship to other approaches, J. Chem. Phys. **73**, 5711 (1980).

[37] R. Winkler, *Spin-orbit Coupling Effects in Two-Dimensional Electron and Hole Systems*, Springer Tracts in Modern Physics, Vol. 191 (Springer, Berlin, Heidelberg, 2003).

[38] L. H. Pedersen, N. M. Møller, and K. Mølmer, Fidelity of quantum operations, Phys. Lett. A **367**, 47 (2007).

[39] J. Simon, F. A. Calderon-Vargas, E. Barnes, and S. E. Economou, Fast noise-resistant control of donor nuclear spin qubits in silicon, Phys. Rev. B **101**, 205307 (2020).

[40] E. Paladino, Y. M. Galperin, G. Falci, and B. L. Altshuler, 1/f noise: Implications for solid-state quantum information, Rev. Mod. Phys. **86**, 361 (2014).

[41] O. E. Dial, M. D. Shulman, S. P. Harvey, H. Bluhm, V. Umansky, and A. Yacoby, Charge Noise Spectroscopy Using Coherent Exchange Oscillations in a Singlet-Triplet Qubit, Phys. Rev. Lett. **110**, 146804 (2013).

[42] Y. Goldin and Y. Avishai, Nonlinear response of a Kondo system: Perturbation approach to the time-dependent Anderson impurity model, Phys. Rev. B **61**, 16750 (2000).

[43] J. Romhányi, G. Burkard, and A. Pályi, Subharmonic transitions and Bloch-Siegert shift in electrically driven spin resonance, Phys. Rev. B **92**, 054422 (2015).

[44] L. S. Theis and F. K. Wilhelm, Nonadiabatic corrections to fast dispersive multiqubit gates involving Z control, Phys. Rev. A **95**, 022314 (2017).

[45] R. Winkler, Quasi-degenerate perturbation theory, in *Springer Tracts in Modern Physics* (Springer, Berlin, 2003), pp. 201–206.